Published in final edited form as:

Nat Neurosci. 2019 September ; 22(9): 1477–1492. doi:10.1038/s41593-019-0452-x.

Zebrafish oxytocin neurons drive nocifensive behavior via brainstem premotor targets

Caroline L. Wee[1,2], **Maxim Nikitchenko**[1], **Wei-Chun Wang**[3], **Sasha Luks-Morgan**[3], **Erin Song**[1], **James Gagnon**[1,8], **Owen Randlett**[1], **Isaac H. Bianco**[1,9], **Alix M. B. Lacoste**[1], **Elena Glushenkova**[1], **Joshua P. Barrios**[3], **Alexander F. Schier**[1,4,5,6,7], **Samuel Kunes**[1], **Florian Engert**[1], **Adam D. Douglass**[3]

[1]Department of Molecular and Cellular Biology and Center for Brain Science, Harvard University, Cambridge, Massachusetts, USA

[2]Program in Neuroscience, Department of Neurobiology, Harvard Medical School, Boston, Massachusetts, USA

[3]Department of Neurobiology and Anatomy, University of Utah, Salt Lake City, Utah, USA

[4]Center for Brain Science, Harvard University, Cambridge, Massachusetts, USA

[5]Broad Institute of MIT and Harvard, Cambridge, Massachusetts, USA

[6]Harvard Stem Cell Institute, Cambridge, Massachusetts, USA

[7]FAS Center for Systems Biology, Harvard University, Massachusetts, USA

[8]Present address: Department of Biology, University of Utah, Salt Lake City, Utah, USA

[9]Present address: Department of Neuroscience, Physiology & Pharmacology, University College London, London, UK

Abstract

Animals have evolved specialized neural circuits to defend themselves from pain- and injury-causing stimuli. Using a combination of optical, behavioral and genetic approaches in the larval zebrafish, we describe a novel role for hypothalamic oxytocin (OXT) neurons in the processing of noxious stimuli. *In vivo* imaging reveals that a large and distributed fraction of zebrafish OXT

Correspondence: Adam D. Douglass, Department of Neurobiology and Anatomy, University of Utah, 20 South 2030 East, Bldg. 570 BPRB, Rm. 480, Salt Lake City, UT 84112, adam.douglass@neuro.utah.edu; Florian Engert, Department of Molecular and Cellular Biology, Harvard University, 16 Divinity Ave, Biolabs 2073, Cambridge, MA 02138, USA, florian@mcb.harvard.edu.

AUTHOR CONTRIBUTIONS:

C.L.W., A.D.D. & F.E. conceived of the project, with critical advice and guidance from S.K., E.S. and M.N. A.D.D. & F.E. supervised the project. C.L.W. designed and performed most of the experiments, and analyzed most of the data. M.N. developed hardware and software for calcium imaging and behavioral experiments, designed and performed some experiments and analyzed the free-swimming behavioral data. W.C.W. & S.L.-M. performed experiments and analyzed data; E.S., O.R., A.M.B.L. & E.G. performed experiments; J.P.B. developed software for behavioral analysis. I.H.B. developed the optogenetic stimulation setup and advised experiments. J.G. and C.L.W. generated the oxytocin CRISPR mutant. A.D.D. and C.L.W. generated the *Tg(oxt:Gal4)* line. A.F.S. supervised J.G., O.R. & A.M.B.L. and advised the project. C.L.W. and A.D.D. wrote the manuscript with contribution from all other authors.

COMPETING INTERESTS

The authors declare no competing interests.

neurons responds strongly to noxious inputs, including the activation of damage-sensing TRPA1 receptors. OXT population activity reflects the sensorimotor transformation of the noxious stimulus, with some neurons encoding sensory information and others correlating more strongly with large-angle swims. Notably, OXT neuron activation is sufficient to generate this defensive behavior via the recruitment of brainstem premotor targets, whereas ablation of OXT neurons or loss of the peptide attenuate behavioral responses to TRPA1 activation. These data highlight a crucial role for OXT neurons in the generation of appropriate defensive responses to noxious input.

INTRODUCTION

Specialized neural circuits that identify perceived threats, such as predators or pain, and drive evasive behaviors are found across all species and may form the basis for complex emotions in humans[1,2]. While many elements of these circuits are context- and species-specific, nociceptive circuits share conserved sensory receptors; these could be used as entry points into elucidating pain-processing mechanisms[3]. However, downstream of peripheral sensory neurons, the central circuits involved in nociception and their interactions with motor networks that drive appropriate responses are still largely uncharacterized[2,3].

Increasing attention has been directed toward the hypothalamic neuropeptide oxytocin (OXT) in the processing of noxious stimuli. While much better-known for its sociosexual and affiliative roles, studies have shown that OXT has anti-nociceptive, anti-inflammatory and anxiolytic properties, and thus could ameliorate the perception of, or behavioral response to, painful or aversive experience[4–6]. For example, a population of around thirty OXT neurons, out of thousands in the rodent hypothalamus, suppresses the activity of spinal nociceptors both directly through spinal projections and indirectly by modulating neuroendocrine release of OXT from other OXT subpopulations[4,7]. A distinct amygdala-projecting subpopulation has also been shown to reduce pain-conditioned fear behaviors[5]. However, recent human studies demonstrated that OXT in fact increases defensive responses to unpredictable electric shocks[8] and acoustic startle stimuli[9], indicating that it might be enhancing, rather than suppressing, defensive behaviors under some circumstances.

To understand these apparently contradictory functional roles, it is essential to determine how noxious stimuli are represented within the OXT population, and to relate these activity patterns to behavioral output. The large size and experimental inaccessibility of mammalian OXT nuclei has made it difficult to address these issues, and few functional recordings of OXT neuronal activity have been made in behaving animals. Fortunately, OXT circuits are remarkably well conserved[10]. In fish, neurons producing isotocin, the ortholog of OXT (commonly referred to in the literature as OXT[11–13]) are mainly located in the neurosecretory preoptic-hypothalamic area (PO), which is homologous to the paraventricular nucleus (PVN), supraoptic nucleus, and accessory nuclei of the hypothalamus in mammals[10,14]. As in mammals, zebrafish OXT neurons project to the pituitary, where OXT is released as a neurohormone, and also send axons to a broad range of neuronal targets throughout the forebrain, hindbrain and spinal cord[11–13,15–17].

Here, we use the larval zebrafish, in which the entire OXT population is both optically and genetically accessible, to dissect the role of OXT neurons in the processing of nociceptive inputs. We show that zebrafish OXT neurons respond in a graded fashion to a range of aversive stimuli, with noxious experience causing the strongest and broadest activation. TRPA1 receptor activation drives both OXT neuron firing and defensive swimming behavior in the form of large-angle tail bends, and both the sensory and motor components of this process are encoded in OXT population activity. Experimental activation of OXT cells or TRPA1 receptors recruits a common network of brainstem spinal-projecting neurons, including but not limited to the escape-promoting Mauthner cell[18], to generate these behavioral responses. In contrast, loss of OXT function or ablation of OXT neurons attenuates TRPA1-evoked behavior. Thus, hypothalamic OXT neurons form an essential part of a sensorimotor circuit for nociception in zebrafish, and might also play a broader role in the processing of aversive stimuli.

RESULTS

Brain-wide activity mapping of nociceptive pathways in zebrafish

To identify brain regions that process noxious information we first utilized a “MAP-mapping” approach that relies on whole-brain imaging of phosphorylated ERK (pERK), as a marker of neuronal activity[19]. We found that the preoptic area (PO) and its neurosecretory target, the pituitary gland, were among a number of areas reliably and selectively activated by mustard oil, electric shock and noxious (37°C) heat (Figure 1a–b). A non-nociceptive but aversive vibrational-acoustic stimulus (dish taps) [18] activated the PO less reliably (Figure 1a–b). Other loci were activated by both noxious stimuli and dish taps, such as the caudal hypothalamus and norepinephrinergic locus coeruleus – suggesting that they might play a more general role in aversion (Figure 1a–b). The norepinephrinergic area postrema was activated both by mustard oil and by food, consistent with its known roles in chemical sensation and food intake regulation[20].

OXT neurons respond in a graded manner to noxious and aversive stimuli

Since OXT neurons are the most numerous cell type in the zebrafish PO[14], we asked if they might play a role in nociception. We performed pERK staining on transgenic fish[13] in which GFP is expressed specifically in OXT neurons in the PO and neighboring posterior tuberculum (PT; Figure 1c–d, Figure S1). Indeed, pERK intensity was elevated in OXT neurons upon stimulation with high-intensity electric shock, mustard oil, and noxious heat (37°C), with noxious heat showing the weakest activation (Figure 2a–c). In contrast, mean pERK activity per fish in OXT neurons was not significantly changed by vibrational–acoustic tap stimuli. We also observed widespread activation of some non-OXT neurons by noxious stimuli, especially in the anterior PO (aPO, Figure 1d, 2a–c). These activated neurons may produce corticotropin-releasing factor (CRF) or arginine-vasotocin (AVT), or could be non-neuromodulatory cell types[14]. However, on average, a higher proportion of OXT neurons were activated by noxious stimuli than their neighbors (Figure 2a–b).

We confirmed these resuts by generating a driver line, *Tg(oxt:Gal4),* and crossing it against a *Tg(UAS:GCaMP6s)* reporter to enable calcium imaging in OXT-expressing cells (Figure

S2h, 3a, S3b). The same fish were exposed to shock, mustard oil, heat, and taps, in order to compare OXT responses across different sensory modalities. OXT neurons were responsive to all of the stimuli tested, although taps elicited responses of the weakest magnitude (Figure 2d, S3). Consistent with our pERK results, shock and mustard oil induced strong and widespread OXT neuron activation, while noxious heat induced intermediate levels of activation, which appeared to be stronger than predicted by pERK. Thus, OXT neurons respond in a graded fashion to a range of aversive inputs, with noxious stimuli causing the strongest and most widespread activation. Notably, there was a high degree of overlap between OXT cells responding to shock, mustard oil and heat, suggesting that multiple noxious inputs can be processed by the same neurons (Figure 2d, S3).

Magnocellular and parvocellular OXT neurons are activated by noxious stimuli

As in mammals, zebrafish OXT neurons comprise a diverse population, which can be broadly divided into magnocellular and parvocellular classes[11,12,21,22]. Magnocellular cells are larger, express higher levels of the OXT peptide and project to the pituitary, where OXT is released as a neurohormone. Parvocellular neurons are smaller, express less OXT and project to other regions of the central nervous system (CNS). In agreement with prior work[11,12], we find that magnocellular cells are located more anteriorly than parvocellular cells, being enriched within the PO (Figure S2).

In both pERK and calcium imaging experiments, there was a strong activation of OXT neurons by electric shock and mustard oil across the entire PO and PT clusters, and weaker but similarly distributed activation by heat (Figure 2c–d, Figure S3a–b), whereas dish taps activated more posterior (likely parvocellular) regions within the PO. Thus, noxious stimuli are potent activators of the zebrafish PO/PT, and appear to recruit a higher percentage of both magnocellular and parvocellular OXT neurons as compared to other non-OXT cells in their vicinity.

TRPA1 activation induces nocifensive behavior in zebrafish

Transient Receptor Potential (TRP) cation channels function as tissue-damage sensors in insects, zebrafish and mammals[23,24]. One major class of TRP ion channels, TRPA1, is activated by mustard oil, other chemical irritants and endogenous products of inflammation, whereas heat acts through the related TRPV1, though they overlap significantly in their expression and functions[25–27]. Since OXT neurons responded most strongly to mustard oil stimulation, we focused on TRPA1-mediated signals in our subsequent characterization of OXT's role in nociception.

As a diffusible stimulus that binds covalently to TRPA1[28], mustard oil is difficult to deliver in a spatiotemporally precise way. To explore the dynamic relationship between TRPA1 channel activation, OXT signaling, and behavior, we took advantage of a small molecule, Optovin[29,30], which can be photoconverted into a TRPA1 agonist in the presence of UV light. After the light is switched off, Optovin reverts to an inactive state within seconds[29,30]. By immersing larvae in Optovin and stimulating the tail with brief pulses of 405 nm light, we could activate TRPA1 in a spatially and temporally controlled manner (Figure 3a).

Optovin-based TRPA1 stimulation consistently elicited tail bends, which were significantly higher in frequency, velocity, and magnitude than the average movement elicited by light in DMSO (Figure 3b, Supplementary Video 1). These large-angle tail bends were also observed after mustard oil and noxious-heat stimulation, suggesting that they are likely a nocifensive response (Figure S3c). The similarity between Optovin-evoked and other forms of nocifensive behavior suggested that we could use this approach to further characterize OXT-mediated sensorimotor processing.

OXT neuron activity is induced by TRPA1 stimulation and correlates with nocifensive behavior

Whereas the mammalian hypothalamus contains thousands of OXT neurons, the larval zebrafish has fewer than 100 (55.0 ± 0.76 (OXT_{PO}), 12.9 ± 0.34 (OXT_{PT}), mean of 83 fish, Figure S2a), making it possible to record the activity of a large fraction of the population and to correlate each neuron's activity with behavioral output. Since a substantial subset (~70%) of preoptic OXT neurons, and occasionally a few neurons in the PT cluster, are labeled by *Tg(oxt:Gal4;UAS:GCaMP6s)* (38.6 ±3.00 neurons (OXT_{PO}), 0.79± 0.3 neurons (OXT_{PT}), mean ± SEM of 14 fish), we were able to combine volumetric two-photon calcium imaging, Optovin-mediated TRPA1 stimulation, and behavioral recordings to simultaneously monitor population-wide OXT neuron activity and nocifensive behavior in real time (Figure 3a).

While we only occasionally observed OXT neuron activation upon stimulation with UV in DMSO, OXT neurons showed strong and synchronous responses to TRPA1 activation that varied with stimulus intensity and correlated with larger and longer-lasting tail movements (Figure 3c). In contrast, UV stimulation in DMSO was associated with a smaller calcium response and lower-amplitude tail movement that was similar across light intensities (Figure 3d). OXT neuron activity was also higher during spontaneous large-angle bouts, suggesting a potential role for OXT neurons in driving motor behaviors in other contexts (Figure 3c–d). The rise in calcium activity on average appeared to slightly precede tail movements, a phenomenon that was most obvious during spontaneous events (Figure 3d).

However, there were also instances of spontaneous large-angle tail bends that were not obviously accompanied by OXT activity, and other instances where OXT activity was not correlated with strong behavioral output (Figure 3c). This diversity of responses in individual cells corresponded not only to TRPA1-stimulus and motor responses, but also to spontaneous and stimulus-induced movements that occurred in DMSO (Figure 3c).

Diversity and distribution of OXT sensorimotor responses to TRPA1 activation

To further probe the diversity of sensorimotor representations within these cells, we generated stimulus and motor regressors, and used them to classify neurons into distinct functional types based on their degree of correlation with the stimulus and/or behavior[31]. The stimulus regressor varied with the absolute UV light intensities presented to the fish in both DMSO and Optovin. To distinguish stimulus-locked and spontaneous motor activity in the OXT population, we generated two types of motor regressors, one that reflected stimulus-locked motor output ($motor_{stim}$ regressor), and another that reflected spontaneous

locomotion occurring in the absence of the stimulus ($motor_{spon}$ regressor). In both DMSO and Optovin, stimulus and motor output (i.e. $motor_{stim}$) were only moderately correlated (r = 0.36±0.03 in DMSO, and 0.67±0.04 in Optovin, Figure S4a), suggesting there was sufficient variability to probe both sensory and motor components of the OXT circuit. We then correlated the activities of all OXT neurons (n = 552 from 14 fish) to the 3 stimulus and motor regressors for both DMSO and Optovin conditions (6 regressors in total), to probe the distribution of sensorimotor representations in noxious and non-noxious contexts (Figure 4a).

As predicted, many more neurons showed significantly stronger correlation with the stimulus and behavior in Optovin (i.e. TRPA1 activation) compared to DMSO (UV light alone), which is reflected by a right-shift in the distribution of correlation coefficients (Figure 4b). In contrast, the correlation of OXT neuron activity with spontaneous behavior was slightly reduced in Optovin versus DMSO, likely because of an increase in small-amplitude forward swims (“tail twitches”) that occurred in some fish after repeated stimulation with Optovin (see Figure 3d for examples).

Across a range of thresholds, the proportion of cells that showed stimulus or motor correlations in Optovin was higher than in DMSO or for spontaneous movements, confirming that OXT neurons predominantly respond to TRPA1 activation (Figure 4c). At a stringent threshold of r = 0.35, which was based on an estimate of spurious correlations (see Figure S4b), we found that 39% of OXT neurons had activity correlated with the stimulus regressor in Optovin, and a lower, partially overlapping proportion (29%) was correlated with post-stimulus motor activity (i.e. $motor_{stim}$ regressor, Figure 4d). In Optovin, the activity of stimulus-correlated neurons tended to parallel stimulus intensity, whereas $motor_{stim}$ related neurons had more variable activity in response to both strong and weak stimuli, and thus might be encoding motor behavior (Figure 4a, f).

In contrast, only 10% of all neurons showed stimulus correlation in DMSO, while 6% showed stimulus-related motor activity, consistent with the observation that most UV stimulations in DMSO resulted in much weaker behavioral responses as compared to in Optovin. We also did not observe UV-related activity in all animals (Figure 4e). Of the small fraction of OXT neurons that were UV-responsive in DMSO, the response magnitude appeared to be much larger, but less sensitive to stimulus intensity (Figure 4f). Since UV is also a mildly aversive and potentially damaging stimulus in zebrafish[32], the observation of UV-induced responses is consistent with a broader role for OXT neurons in encoding negative inputs. We also found cells that were active both in DMSO and Optovin (Figure 4d, S4c). It is possible that these cells continue to encode the UV stimulus in Optovin, or are multimodal cells that are also tuned to TRPA1 stimulation.

Notably, some OXT neurons had activities that were correlated with spontaneous tail bends, suggesting that OXT neuron activity is not simply evoked by the UV/TRPA1 stimulus, but may also have an independent motor function. It is possible that a subset of these ‘spontaneous’ movements reflect behavioral responses to the heat of 2P laser stimulation, since they often occurred at the onset of 2P laser scanning (see Figure 3d). Consistent with this idea, a majority (60%) of OXT neurons that fired in correlation with spontaneous

movements in DMSO or Optovin also tended to be activated by TRPA1 stimulation (Figure 4d, S4c).

Similar to our pERK and other calcium imaging results, TRPA1 stimulus or motor-related neurons were highly intermingled and distributed throughout the population (Figure 4f–g), with a slight enrichment of TRPA1 stimulus-related neurons in the aPO relative to motor-related and UV-responsive neurons. Since we strictly controlled for the area of stimulation, it is unlikely that this distributed pattern is a function of receptive field location.

To determine whether nociceptive responses are unique to OXT neurons or are a general property of cells in the PO or PT, we also repeated our TRPA1 stimulation and *in vivo* imaging experiments in a pan-neuronal GCaMP6s line (*Tg[HuC:GC6s]*) co-expressing *Tg[oxt:Gal4;UAS:nfsb-mCherry]*) to define OXT and non-OXT populations, and compared the activities of these groups in the same fields of view (Figure S5–6, n = 13 fish). Similar to our pERK results, OXT neurons were more strongly activated by TRPA1 stimulation than non-OXT neurons, whereas activity observed during spontaneous movements and UV stimulation were more similar between the two groups (Figure S5–6).

In summary, OXT neurons comprise a highly diverse and functionally heterogeneous population of cells with variable roles in the sensory and motor components of nociceptive and aversive signaling. A significant subset shows activity locked to defensive behavior, raising the possibility that OXT may contribute to behaviors caused by TRPA1 receptor activation.

Optogenetic activation of OXT neurons drives large-angle tail bends

To determine if OXT neurons play a role in driving locomotor responses to noxious stimuli, we expressed channelrhodopsin (ChR2) in OXT neurons using *Tg(oxt:Gal4; UAS:ChR2-EYFP)* fish (Figure 5a). Focusing spatially-restricted blue light onto ChR2-positive OXT_{PO} neurons evoked strong swimming behavior (Figure 5a–c, Supplementary Video 2). Behavior could also be elicited by stimulating free-swimming eyeless fish (Figure 5i, j) but not sibling controls that lacked ChR2 expression (Figure 5d–e), demonstrating that the behavior was not visually evoked. However, stimulus durations on the order of seconds were required in order to achieve a high probability of response (Figure 5b–e), and the mean latency to behavior onset was relatively long (1.8 ± 0.13 s for 5 s stimulus, Figure 5f–g, k). Response frequencies and latencies were also highly variable (Figure 5c, f–g, k). Because we used high light intensities (6 mW/mm^2) that were sufficient to activate other neurons at much shorter latencies (Figure S7a), it is unlikely that the long lag and variability of OXT-evoked behavior is due to insufficient illumination. Since even in stable transgenic fish we rarely observed ChR2 labeling in more than 25 OXT_{PO} neurons per animal (i.e. ~50% of the population, Figure S7d–e), and only a subset of these neurons might encode motor output, it is possible that a longer stimulation period is required to recruit sufficient neurons to drive behavior. Furthermore, OXT-containing vesicles might only be released upon prolonged stimulation, which might in a more naturalistic scenario be necessary for reducing response latencies[5,21,33]. Using mosaic labeling, we found that the probability and frequency of optogenetically-induced swimming strongly correlated with the number of OXT_{PO} neurons expressing ChR2 (Figure S7d–e). Notably, we were able to optogenetically induce

swimming even in fish that had few or no pituitary projections (Figure S7e). Thus, it is likely that this behavior is mediated, at least in part, by parvocellular OXT neuron projections to the hindbrain/spinal projections.

Similar to TRPA1 receptor activation, tail bends induced by OXT neuron stimulation were greater in magnitude and kinematically distinct from C-bends induced by taps, acoustic startle, or optogenetic activation of somatosensory neurons (Figure 5h, S7a–c, S8). Thus, instead of specifically activating classical predator escape reflex circuits identical to those driven by milder aversive stimuli[18], OXT might modulate a distinct or partially overlapping network that promotes a faster and larger-angle motor output in response to noxious stimuli.

Role of the neuropeptide OXT in driving large-angle tail bends

As in mammals[34,35], we found that zebrafish OXT neurons co-express glutamatergic markers (Figure 6a), raising the question of the relative contributions of OXT itself versus other neurotransmitters in driving defensive behavior. To address this question, we first asked if OXT applied directly to the exposed hindbrain and spinal cord was sufficient to drive large-angle tail bends. Fish were transected at the midbrain/hindbrain boundary, and all tissue anterior to the hindbrain, including the OXT neurons, was removed. Beginning at about 5 minutes after bath application of OXT, we observed a large burst of swimming activity comprised mostly of large-angle tail bends (Figure 6b–d, Supplementary Video 3–4). These results suggest that the peptide OXT can act directly on hindbrain/spinal circuitry, and is sufficient, even in a reduced preparation, to drive behavior that resembles nocifensive responses.

We next asked whether OXT was necessary for ChR2-induced behavior. To that end, we used the CRISPR/Cas9 system to generate OXT-null mutant zebrafish, and identified a 575 bp deletion predicted to be a null allele (Figure 6e). We then compared the effect of optogenetically stimulating OXT neurons in OXT null mutants and their heterozygous siblings (Figure 6f, S9a–b). While the absence of OXT did not completely abolish ChR2-evoked swimming behavior, it significantly reduced its probability, frequency, and response latency. There were no observable differences between wild-type and heterozygous OXT mutants (Figure S9c). Thus, the absence of OXT attenuates the efficacy of OXT neurons in driving locomotion.

Taken together, these results suggest that although the peptide OXT is sufficient to drive large-angle tail bends, OXT neurons possess functionally redundant mechanisms, likely involving co-expressed neurotransmitters, which can partially compensate for the absence of OXT. We propose glutamate as the most likely candidate for supplying this excitatory locomotor drive[36].

Brainstem reticulospinal neurons are downstream targets of TRPA1 and OXT neuron activation

To identify the neuronal targets by which OXT elicits defensive behavior we focused on the reticulospinal system[37], a highly stereotyped population of approximately 250 spinally-projecting motor command neurons that we found to be densely innervated by *Tg(oxt:GFP)*-expressing axons (Figure 7a). Calcium imaging of the reticulospinal array during either

ChR2 or Optovin stimulation allowed us to identify cells that are activated downstream of OXT neuron activation or nociceptor signaling. We found that both TRPA1 activation and *Tg(oxt:Gal4; UAS:ChR2-EYFP)* stimulation activated a common subset of these cells, including the Mauthner cell (M-cell) and several other premotor targets (RoM2, RoM3, RoL3, MiV1, MiV2; Fig. 7a–d). Evoked calcium signals in these neurons reliably preceded fictive motor bursts recorded by EMG (Figure 7b–d). The probability of activation for each reticulospinal cell type was strikingly similar between TRPA1 stimulation and optogenetic OXT activation, suggesting overlap between these pathways.

The M-cell is a crucial component of zebrafish escape circuitry[18,38,39]. While the kinematic differences between TRPA1/OXT-driven behaviors and other forms of escape suggested differential reliance on downstream targets, our observation that one of the two M-cells were activated during roughly 50% of Optovin and ChR2 trials (Fig. 7c) led us to ask if they might play a similarly important role in shaping the properties of nocifensive behavior. To that end, we bilaterally ablated both M-cells and measured behavioral responses to both TRPA1 and optogenetic OXT stimulation (Figure 7e). The majority of behavioral parameters, including response probability, frequency, maximum bend angle, velocity, and duration were unaffected by M-cell ablation relative to sham ablated controls (Figure 7f, Figure S10). The only exception was behavioral latency, which was significantly increased for optogenetically- but not Optovin-evoked swimming (Figure 7g, S10; ChR2: Mean increase = + 360.9 ± 104.7 ms, *p = 0.03; Optovin: Mean increase = −192.7 ms ± 76.5 ms, p = 0.062 (N.S.)). The differential effects on latency might reflect a lower degree of complexity in the neuronal signals elicited by ChR2 activation versus more naturalistic sensory stimuli. Overall, we conclude that the characteristic features of TRPA1 and OXT-induced behavior do not absolutely require the M-cell and are instead relayed to the spinal cord through the parallel activation of multiple reticulospinal targets.

Loss of OXT function attenuates behavioral responses to TRPA1 stimulation

To determine if the OXT circuit was necessary for the implementation of nocifensive behavior, we used Optovin to photochemically activate TRPA1 receptors in free-swimming larval zebrafish (Figure 8a). As with restrained fish, TRPA1 stimulation strongly increased locomotor output by eliciting large-angle tail bends (Figure 8b, Supplementary Video 5–6). Due to limitations of our behavioral setup we were not always able to perfectly resolve tail angles in those experiments, and thus used velocity changes as a more reliable behavioral metric.

We chemogenetically ablated OXT neurons in transgenic *Tg(oxt:Gal4;UAS:nitroreductase-mCherry)* fish by treatment with metronidazole (MTZ), a pro-drug that is enzymatically converted into a toxic product by nitroreductase to cause cell-specific ablation (Figure S11). Since *Tg(oxt:Gal4;UAS:nitroreductase-mCherry)* has variegated expression, this manipulation likely only ablates about 50-75% of the OXT population (Supplementary Table 1). Despite this caveat, partial ablation with MTZ (starting from 5 dpf) also significantly reduced responses to TRPA1 stimulation, relative to MTZ-treated control siblings lacking nitroreductase (Figure 8e). There were no differences in light responses while in DMSO. In Optovin, the median post-stimulation increase in swim speed was 35% lower in OXT

neuron-ablated fish than for control siblings. Furthermore, ablation of OXT neurons did not affect baseline swim kinematics, suggesting that the effects of our manipulation were specific to nocifensive behavior (Figure 8f).

We next asked whether genetic deletion of OXT (which attenuated OXT neuron-evoked locomotion (Figure 6f, S9a–b)) similarly reduced TRPA1-activation-induced behavior. We compared the behavioral responses of *oxt−/−* null mutants to their heterozygous siblings. Loss of OXT significantly attenuated light-evoked behaviors in Optovin-treated fish (Figure 8c), while no differences between genetic groups were observed in DMSO control trials. In Optovin, the median post-stimulation increase in swim speed was 38% lower in *oxt−/−* null mutants compared to heterozygous siblings (Figure 8c), similar to the effect observed with OXT neuron ablation. Deletion of OXT also did not affect baseline swim kinematics, suggesting that the reduction in TRPA1-induced behavior was not due to a gross locomotor deficit (Figure 8d). Taken together, these experiments demonstrate that OXT neurons contribute to driving the behavioral response to noxious stimuli.

DISCUSSION

Using *in vivo* imaging of OXT population activity in zebrafish, we describe a multimodal neuromodulatory circuit that is involved in the sensorimotor transformation of nociceptive signals. A large and distributed fraction of hypothalamic OXT cells respond strongly to noxious inputs, including TRPA1 stimulation, and more weakly to other aversive stimuli. While some neurons are tuned specifically to sensory stimuli, others display behaviorally-correlated activities, which together with gain and loss-of-function experiments implicate OXT in the generation of nociception-triggered motor output via activation of brainstem premotor targets. Our results strongly support a conserved role for OXT in nociceptive processing, and suggest diverse functions for OXT circuits in both the integration of sensory input and the generation of defensive locomotor responses.

Extensive activation of OXT neurons by noxious and other aversive stimuli

While previous mammalian studies identified small, ostensibly specialized subpopulations of OXT neurons that may be involved in pain or fear processing[4,5,10], it has been unclear whether these subgroups are unique or ubiquitous. Here, through population-level activity recordings in behaving zebrafish, we show that a large percentage OXT neurons, likely spanning both parvo- and magnocellular types, acutely respond to noxious stimuli.

The extent of OXT activation by a particular aversive stimulus appears to scale with the potential for damage. Notably, OXT neurons responded to aversive but non-nociceptive “startle” stimuli, such as taps and UV flashes, but to a lesser degree than for TRPA1 activation or noxious heat. Interestingly, the magnitude and extent of the OXT signals elicited by non-noxious stimuli varied dramatically between animals, suggesting potential modulation by other factors such as prior exposure to noxious stimuli, contextual cues or internal state.

It is likely that OXT acts in concert with other closely apposed cell types such as CRF or AVT-expressing neurons[14,35,36,40], which have similarly been implicated in pain and stress

behaviors. In both zebrafish and mammals, OXT may form part of a larger paraventricular "stress response" network, which together with other brain regions such as the locus coeruleus, area postrema, and caudal hypothalamus, coordinates defensive behavior against noxious and other threatening stimuli[41,42].

Oxytocin neurons drive defensive locomotion via reticulospinal circuitry

A small number of previous studies suggested a locomotor role for OXT using pharmacological manipulation of reduced preparations**.** However, the functional relevance of such observations was unknown, or speculated to be related to reproductive behaviors[43–45]. Our finding that OXT (and OXT neuron activation) can drive large-angle tail bends directly links the *in vivo* activity of OXT neurons to defensive locomotion. These behaviors are kinematically distinct from the startle responses that are elicited by the threat of predation, suggesting the evolution of distinct mechanisms for escaping the potential for harm (i.e. predator approach) versus actual physical harm, similar to what has been proposed in mammals[2]. Such distinctions appear to be mediated by a differential reliance on hindbrain premotor neurons. While the M-cell is considered to be an essential component of the startle response, it responds less reliably than other premotor cells to TRPA1 or OXT stimulation, and its ablation has few consistent effects on evoked behaviors. Thus, we infer that the M-cell's contribution to the unique characteristics of OXT- and TRPA1-evoked swimming is minimal or redundant with other OXT targets.

Our data also suggest that the OXT neurons' ability to recruit reticulospinal targets relies on the co-release of both OXT peptide and other neurotransmitters, such as glutamate. Although OXT itself is sufficient to induce large-angle tail bends, genetic deletion of OXT only partially impairs optogenetically-induced locomotion and nociceptive behavioral responses. While the purpose of such functional redundancy is still unknown, the OXT peptide has previously been shown to facilitate to synaptic transmission, sharpen spike timing and increase the robustness of spike transmission, and thus may be important for modulating the latency, precision or intensity of defensive locomotor behaviors[46]. OXT co-release could exert more sustained effects on hindbrain/spinal circuitry through sensitization and synaptic plasticity[47]. Additional approaches, such as patch-clamp recordings of identified locomotor targets and cell-specific genetic perturbation of glutamate biosynthesis will be required to confirm this hypothesis.

Oxytocin circuit function across evolution

OXT is most often characterized as a pain and fear-reducing molecule that attenuates behavioral responses to threats, yet it has also been shown to enhance fear, pain and defensive responses in rodents and humans[6,8,9,48]. Our data show that these "behavior activating" effects of OXT should be considered alongside the anxiolytic, anti-nociceptive and anti-inflammatory functions that have been demonstrated by other studies[4]. While OXT is sufficient to drive defensive locomotion in zebrafish, it could simultaneously be playing an anxiolytic or analgesic role For example, one recent paper showed that direct and persistent activation of TRPV1 nociceptors by OXT leads to receptor desensitization and analgesia over the long term[49]. Indeed, our discovery of both sensory and motor-related cell types that

span both magnocellular and parvocellular OXT populations is suggestive of multiple integrative pathways being triggered in parallel.

The locomotion-enhancing effects of OXT in mammalian spinal preparations, overall conservation of OXT neuroanatomy and expression of OXT receptors within mammalian spinal circuits[50] all suggest that OXT's role in motivating defensive behaviors could be conserved in other vertebrates, even if precise motor targets and behavioral output differ between species[1]. Overall, our study highlights how neural pathway dissection in the larval zebrafish model can be used to characterize sensorimotor transformations within neuromodulatory populations, and complement mammalian studies in demonstrating the sufficiency of hypothalamic activation for the execution of fundamental defensive behaviors.

METHODS

Fish Husbandry

Larvae and adults were raised under standard conditions and maintained on a 14:10 hr light:dark cycle at 28°C. All protocols and procedures involving zebrafish were approved by the Harvard University/Faculty of Arts & Sciences Standing Committee on the Use of Animals in Research and Teaching (IACUC) and by the University of Utah IACUC. All larvae were raised either in facility water or embryo water (0.6g Instant Ocean in 2L RO water, add bicarbonate to pH 7.2) and fed with an excess of paramecia daily starting from 5dpf. All experiments were performed between 6 – 8 dpf.

Transgenic lines

The following transgenic lines were used in the study:

Tg(oxt:GFP) [13] (E. Glasgow, Georgetown University);

Tg(oxt:Gal4) [Tg(oxtl:gal4-vp16)] (generated for this study by A.D.D., F.E. and C.L.W.);

Tg(HuC:GCaMP6s) [Tg(elavl3:GCaMP6s)a13203)] [51] (F.E.);

Tg(UAS:GCaMP6s) [52] (K. Kawakami, NIG, Japan);

Tg(UAS-E1b:NTR-mCherry) [53] (available from ZIRC); *Tg(Vglut2a:dsRed)* [54];

Tg(UAS:ChR2-YFP) [55] (A.D.D., F.E.); *Tg(UAS -E1b:Kaede)* [56]; *Tg(isl2b:Gal4)* [57]

All above lines were maintained in the AB background. For imaging experiments requiring unpigmented fish, the *mitfa (nacre)* mutation was introduced to these transgenic lines.

The *Tg(oxtl:gal4-vp16)* line [referred to as *Tg(oxt:Gal4)]* was generated by PCR amplifying the 2.1 kb *oxt* enhancer sequence described by Coffey et al., 2013[13], incorporating attB1//B2 sites, and then inserting it into the Gateway pDONOR vector via BP reaction to make pENTR:2.1oxt. This entry clone was then LR reacted against pDest-Tol2:gal4-vp16 to create the expression construct. The resulting plasmid was co-injected into 1-cell stage, *Tg(UAS:nfsbCherry)*-expressing embryos (AB background) at a concentration of 30 ng/μL

with Tol2 transposase mRNA at a concentration of 30 ng/μL. A single founder was selected based on high and uniform levels of expression. The degree of expression mediated by the *Tg(oxt:Gal4)* line is dependent on the specific UAS transgene used, as summarized in Supplementary Table 1.

Generation of oxt mutant using CRISPR/Cas9

Ten Cas9 target sites within the *oxt* open reading frame were chosen using CHOPCHOP[58] to generate short guide RNAs (sgRNA) for mutagenesis. The DNA sequences used to create these sgRNAs are shown below. Cas9 protein was mixed with all ten sgRNAs and injected into embryos at the 1-cell stage[59]. Clutches from outcrosses of these injected fish were screened by PCR using flanking primers and Sanger sequencing to identify a 575 bp deletion allele. Founders were outcrossed repeatedly to reduce the likelihood of unlinked, off-target mutations affecting the *oxt*−/− genotype. Lack of *oxt* expression was confirmed by immunostaining with an anti-oxt antibody (see Figure 6). Mutant fish were genotyped using a three primer PCR-based strategy. This mutant can be obtained from Dr. Adam Douglass (Univ. of Utah).

List of CRISPR guideRNAs: oxt_target1: GTCTGGAGGTCTGCTGTCCGCGG

oxt_target2: TGGAGGTCTGCTGTCCGCGGCGG

oxt_target3: TGGGGCCGAAACAGCGTCCGCGG

oxt_target4: AGAAACCCTGCGCTGCCTGGAGG

oxt_target5: GAGATGTCTGGAAAGGCCTGCGG

oxt_target6: TGGAAAGGCCTGCGGTTATGAGG

oxt_target7: TGTCTCAGAGGGCTGCAGTGTGG

oxt_target8: GGATTCTAGAGGGGTGTGCGTGG

oxt_target9: GTGTCTGCTGTCCGTCTGCTCGG

oxt_target10: GATGTAGCAGGCCGAGCAGACGG

List of oxt genotyping primers: oxt_flanking_PCR_F: CTCTTCCTCCACAGTAATGTCTGG

oxt_flanking_PCR_R: CTCCTGAGATGATGTCACAGCTC

oxt_genotyping_PCR_F: ACAAGACACAAACACTAAGTAAGCATG

oxt_genotyping_PCR_deletionR: GGCAAGTCATTGTATAACAGTGGTTTG

oxt_genotyping_PCR_wildtypeR: GGCAGTTTGAGATGTAGCAGG

Whole brain MAP-mapping experimental protocol

7dpf larvae were divided evenly into control and treatment groups in 85 mm dishes and exposed to experimental stimuli. The protocols for optomotor and aversive stimuli (taps, electric shock, heat) were previously published in Randlett et al (2015)[19]. They are as follows: 1) Electric shock: ~3V/cm, once every 10s for 15 min; 2) Taps: suprathreshold tap once every 10 seconds for 15 min; 3) Mustard oil: 10 or 25 μM in 0.1% DMSO for 15 min; 4) Heat: 37°C water bath for 15 min. In data shown in Figure 2, the interstimulus interval for shock and taps was increased to 30 seconds to reduce desensitization, and 2 different shock intensities were tested. We also added a 40°C degree heat treatment (15 min). Other protocols remained identical.

For the food stimulus, paramecia were added to a dish of larvae that had been food-deprived for 2 hrs, while paramecia water was added to the control. For cocaine treatments, fish were exposed to 1 μM cocaine-HCL (Sigma) or solvent (water) control. After 45 min (cocaine) or 15 min (all other stimuli), larvae were funneled through a sieve and then quickly dropped into 4% paraformaldehyde, immunostained, imaged and analyzed as in Randlett et al (2015).

High resolution (0.8/0.8/2 μm voxel size) confocal images of individual brains were then acquired and registered to a reference brain (x/y/z = 621/1406/138 voxels). Registered images were then downsampled (x/y/z = 300/679/80 voxels; 1.6/1.6/3.5μm voxel size), and statistical comparisons were made at each voxel by calculating a Z-score between treatment and control. To set a false discovery rate (FDR) threshold, pseudogroups were assembled containing an equal number of randomly assigned fish from “control” and “treatment”, and a Z score is calculated as before. We then set a FDR threshold of 0.00005, indicating a 0.005% probability of finding a value greater than this threshold in the pseudogroup comparison. The Z scores for the real data were then thresholded at this value of Z, and suprathreshold voxels were assigned an intensity equal to the difference in the median values of the groups.

Automated quantification of high-resolution pERK data

For quantification of pERK/tERK ratios in individual OXT neurons, pERK experiments were performed on dissected *Tg(oxt:GFP)* fish, mounted in glycerol ventral-side-up on glass slides. High-resolution, tri-color (GFP, pERK and tERK) images were acquired on a confocal microscope (Olympus FV1000), and cellular data was automatically extracted using custom Fiji (ImageJ)[60] and MATLAB software that will be made available online (see Figure S1). The process involves: 1) ImageJ: cropping and reducing images to a specific region-of-interest (in this case, spanning the entire OXT PO and PT populations); 2) ImageJ: extracting individual particles (i.e. cells), using either an inverted and processed tERK image, or directly from the GFP channel; 3) MATLAB: Quantification of activity based on extracted pERK/tERK ratios from both OXT and non-OXT cells; 4) MATLAB: Normalization of pERK/tERK ratios (to the mean of control groups) and aggregation of data across multiple experiments to increase sample sizes. For Figure 2c, we plotted cells that exceeded a threshold above which only 3% of oxt:GFP-positive cells in the control group would be considered active. The same threshold was then applied to non-OXT cells.

Immunohistochemistry (for MAP-mapping and anti-oxt immunostaining)

After 24 hours of fixation with 4% paraformaldehyde (PFA) in PBS + 0.25% Triton (PBT), fish were washed in PBT, incubated in 150mM Tris-HCl, pH 9 for 15min at 70°C, washed in PBT, permeabilized in 0.05% Trypsin-EDTA for 45min on ice, washed in PBT, blocked in blocking solution (10% Goat Serum, 0.3% Triton) for at least an hour and then incubated in primary and secondary antibodies for up to 3 days at 4°C in blocking solution. In between primary and secondary antibody treatments, fish were washed in PBT and blocked for an hour. For higher-resolution images, fish were dissected 24 hours post-fixation, not permeabilized in Trypsin-EDTA prior to staining, and mounted in glycerol on glass slides.

For immunostaining against oxytocin, we used either a commercial rabbit anti-oxytocin (Used in Figure 6, AHP371, AbD Serotec (now BioRad), 1:300); or a rabbit anti-oxytocin (Used in Figure S2, VA10, 1:5000)[61] from Dr. Harold Gainer's laboratory (NIH, Bethesda, USA). Rabbit anti-pERK and mouse anti-ERK (tERK) antibodies (Cell Signaling, #4370 and #4696) were both used at 1:500[19]. Secondary antibodies conjugated with Alexa Fluor dyes (Life Technologies) were diluted 1:500.

In situ hybridizations

For in situ hybridization, brains were fixed in 4% paraformaldehyde + 5% sucrose, dissected out and processed according to the protocol in Thisse and Thisse (2008)[62]. Oxytocin probe was generated by PCR amplification from zebrafish cDNA with the primers CTCCGCAAGCTCTCGGTGTC (fwd) and CTGCACTAATGTACAGTCAAGC (rev), TA cloning the resulting product into pGEM-T, and in vitro transcription (mMessage mMachine SP6, Thermo Fisher). Following development with a BCIP reagent, brains were mounted in glycerol and imaged on an Olympus (BX51WI) compound fluorescence microscope.

Calcium imaging by confocal microscopy

7-8 days-post-fertilization (dpf) larvae of the *mit1fa−/−* (nacre) background expressing *Tg(oxt:Gal4;UAS:GCamP6s)*, were embedded in 1.5% agarose (6 cm dish) with their tails freed. They were imaged at 1 frame per second (fps) on an upright confocal microscope (Olympus FV1000). For all experiments, a single plane covering the largest number of OXT neurons was imaged. Taps were delivered by striking the imaging platform with a solenoid (Guardian Electric 28P-I-12D). Shocks (100ms, 36V) were delivered across a 6cm dish (~=6V/cm) using a Grass stimulator, with the anode and cathode placed near the head and tail of the fish, respectively. Heat was delivered using a heating coil positioned close to the tail of the fish (4V, ~2A, ~2Ω). A 10s heat stimulus was presented, achieving noxious temperatures of ~37°C (peak temperatures may be higher), following which the water temperature was allowed to cool naturally (~5 min to return to room temperature). After > 5 min of heat presentation, mustard oil was pipetted into the dish to achieve a final concentration of 25 μM. Calcium activity was analyzed similarly to 2-photon data (see below). The maximum calcium response within 60s of heat or mustard oil stimulus was used to quantify neural responses, whereas tap and shock responses were aligned based on stimulus onset.

Behavioral recordings were performed on separate fish using the same stimulation methods. Uniformly distributed points along the tail of the fish were extracted online at 100 fps using custom LabVIEW software, and cumulative tail angles analyzed and plotted analyzed in MATLAB.

Simultaneous 2P calcium imaging and behavior during Optovin stimulation

7-8 dpf larvae homozygous for the *mit1fa* (nacre) allele, expressing *Tg(oxt:Gal4;UAS:GCamP6s)*, or co-expressing *Tg(oxt:Gal4;UAS:nfsb-mCherry)* and *Tg(HuC:GCaMP6s),* were embedded in 1.5% agarose with their tails freed. We raised and performed all experiments in embryo water maintained at pH 6.5-7.5, which is crucial for ensuring optimal behavioral responses to TRPA1 stimulation. For volumetric 2P imaging experiments, an electrically tunable lens (Edmund Optics, 83-922) was installed in the light path before the galvanometer scanner to allow fast axial refocusing of the two-photon excitation spot. Images alternating between two or three z-planes per fish were acquired at a frame rate of ~237 ms per z-plane, corresponding to ~474 ms or ~711 ms per z volume respectively. For TRPA1 photoactivation, fish were stimulated first in DMSO (0.1%), then in Optovin (Tocris 4901, 25 μM in 0.1% DMSO, vortexed and filtered with a 0.45 μm syringe filter to remove undissolved particles). For both conditions, fish were first incubated in the respective solutions for 5-10 min.

In both DMSO and Optovin trials, the tail of the fish was stimulated for 100ms with a 405 nm laser at 120 s intervals. The laser was focused on the middle of the tail (1 or 7 mW at sample for low or high intensity stimulation), and aligned on *non-experimental* fish prior to starting the experiment to prevent unnecessary UV exposure in the experimental animals. Long (seconds to minutes) exposure to high intensity UV laser was observed to abolish/reduce OXT neuron responses to TRPA1 stimulation in some fish, possibly due to UV-induced tissue damage. An electronic shutter (Uniblitz VS25) was installed above the objective to prevent PMT saturation by the UV laser. Tail movements were simultaneously monitored under IR (850 nm) illumination at 200 fps (Pike F-032 camera, Allied Vision Technology) through a substage optical path, and tail coordinates were extracted online using custom LabVIEW software.

Calcium imaging analysis

All calcium imaging data was analyzed using custom ImageJ and MATLAB software. The general protocol for analysis was 1) Image registration to correct for motion artifacts using the TurboReg plugin[63] in ImageJ; 2) Extraction of fluorescence signals from both channels using manually-segmented ROIs in MATLAB; 3) Calculation of Δf/f signals from raw traces and alignment to tail traces, as needed, in MATLAB.

For fish expressing *Tg(UAS:GCaMP6s)* exclusively in *oxt*-expressing neurons, ROIs were drawn over all visible cells in a maximum projection image for each plane and raw fluorescence traces were extracted as the mean pixel value within the ROI. For measurements in *Tg(oxt:Gal4;UAS:nfsb-mCherry; elavl3:GCaMP6s)* triple-transgenics, ROIs corresponding to OXT neurons were segmented in the red channel and used to extract fluorescence traces from the aligned green channel. The same neurons were selected in

DMSO and Optovin trials. To measure responses from non-OXT neurons, ROIs were drawn over all visually distinguishable GCaMP neurons in the green channel. Δf/f values were calculated from raw traces using the average fluorescence over the time period before the first stimulus as the baseline to which all traces were normalized.

Regressor analysis

To cross-correlate neuron activity with behavior, we generated regressors from 6 variables - 2 stimulus variables (DMSO and Optovin) and 4 motor variables corresponding to motor behavior that occurred either within 10s post-stimulus, or at all other time points, again for both DMSO and Optovin. The regressors were convolved with a GCaMP6s kernel based on its measured response delay (0.48 s) and decay time (3s, based on Chen et al. (2013)[64]) and cross-correlated with calcium traces that had been smoothed with a 3-frame zero phase filter. We set a positive threshold of r = 0.35 to identify “active” neurons, and a negative threshold of r = −0.35 to identify neurons with anti-correlated activities, though we did not observe the latter in our analysis. These thresholds were set based on the distribution of r-values obtained from mCherry-expressing OXT neurons, which estimates the probability of spurious correlations (i.e. false positives) caused by motion or other artifacts (see Figure S4b).

Optogenetic locomotion experiments

6-8 dpf larvae were embedded in 1.5% agarose with their tails freed, then stimulated using a fluorescence microscope (Olympus BX51WI) equipped with a 40x water-dipping objective. The stimulation area was 150 μm in diameter (A-stop open, F-stop closed), as visualized by Kaede photoconversion (Figure 5a). The light intensity at the sample was calibrated to be 6 mW/mm^2. Fish were stimulated for durations of 0.1, 1, 2, 3 and 5s every 30 s (6 presentations each, randomly shuffled for each fish). OXT mutant clutches were tested using the same protocol and genotyped post-hoc.

For free-swimming optogenetics experiments, 6dpf larvae were lightly anesthetized in 0.1% MS-222 and the eyes were surgically removed using forceps. Fish were returned to warmed Ringer’s Solution and allowed to recover for 12 hrs. Behavioral experiments were performed with the fish placed singly into a 1-inch diameter agarose arena. This arena was placed onto a platform covered with diffusion filter paper, above a blue LED (SP-08-B4, Luxeon) for ChR2 activation and illuminated with an array of 800 nm LEDs. A custom LabVIEW program was used to control data acquisition and stimulus delivery. Fish location was tracked in MATLAB. Ratios of distance traveled during the 5s pulse divided by the total distance traveled during the pulse plus 5 s baseline period were measured for each fish.

Reduced Preparation

7 dpf larvae of the WIK background were embedded in 1.5% agarose in zebrafish ACSF with tails released. A thinned tungsten wire was used to transect the brain above the midbrain/hindbrain boundary. Lack of responses to gentle touch stimuli on the head (at locations anterior to the cut) was used to establish that all forebrain/midbrain tissue had been severed. Transected fish survived for hours in culture solution and produced frequent bouts of small amplitude tail twitches, possibly due to reduced inhibition of hindbrain

reticulospinal circuitry. We waited at least 5 min after commencement of movement before beginning to record baseline tail movements, and pipetted OXT (Tocris Biosciences, 1910) to a final concentration of 5 μM, 10 min after the start of recording. Uniformly distributed points along the tail of the fish were extracted online at 100 fps using custom LabVIEW software, and cumulative tail angles were analyzed and plotted analyzed in MATLAB.

Calcium imaging of reticulospinal neurons

Zebrafish larvae were backfilled from the spinal cord at 4 dpf with 10 % w/v Cal-590 (dextran conjugate 3,000 MW, AAT Bioquest) to label reticulospinal neurons with the red calcium dye. Experiments were performed using 5-7 dpf zebrafish larvae after Cal-590 backfill. Zebrafish larvae were immobilized in 0.1% w/v α-bungarotoxin or 10% formamide and then stabilized on a sylgard-lined glass bottom dish containing extracellular solution (composition in mmol/l: 134 NaCl, 2.9 KCl, 1.2 $MgCl_2$, 2.1 $CaCl_2$, 10 HEPES, 10 glucose, adjusted to pH 7.8 with NaOH). The brain was dissected out to remove all sensory inputs from the head with the connection to the spinal cord preserved.

Calcium imaging was performed using an upright microscope (BX51WI, Olympus) with a sCMOS camera (Zyla, Andor DG-152X-C1E-Fl) and a mercury arc lamp (X-cite 120, Excelitas). Calcium responses of the reticulospinal neurons were acquired with Solis Software (Andor) at 5-20 fps and analyzed with ImageJ and Excel. EMG or motor nerve activity recordings were acquired simultaneously with calcium imaging at 50 kHz with a MultiClamp 700B amplifier, digitized with a DigiData 1550B, and analyzed using pClamp 10 software (Molecular Devices) and Dataview (University of St Andrews). The recording electrodes were made with standard wall glass capillaries with a pipette puller (PIP6, HEKA) and the tip was cut to make a 20-50 mm opening. For TRPA1 stimulation experiments, wild type zebrafish larvae were used and Optovin was added into the extracellular solution in the recording dish with a final concentration of 25 μM. A 410 nm violet LED (20-100 ms, 11.7 mW) was used to activate Optovin-mediated TRPA1 channel opening. To activate oxytocin neurons, *Tg(oxt:Gal4;UAS:ChR2-YFP)* zebrafish larvae were used and a 480 nm blue LED (5 s, 2.4 mW/mm^2) was used to activate the ChR2.

M-cell ablations and behavioral analysis

5-6 dpf fish were anesthetized with MS-222 and backfilled by injection of Texas Red Dextran (ThermoFisher #D3329) into the spinal cord. Fish were then allowed to recover overnight in Ringer's solution at 37°C. The next day, fish were lightly anesthetized with tricaine before being placed onto a 2-photon microscope. Mauthner cells were bilaterally ablated using a mode-locked laser (920 nm) as described in Orger et al., 2008. For sham ablations, the same procedure was followed except the reticulospinal array was not backfilled, and the laser was scanned on an unlabeled section of brain. Tethered behaviors were evaluated before and 1 hr after ablation by imaging at 604 Hz using custom LabVIEW software (Version 16.0, National Instruments). For Optovin trials, a 500 ms pulse of 405 nm light (0.41 mW/mm^2) was used to stimulate the fish's tail. For optogenetic experiments, the same spot of 405 nm light was aimed at the head of the fish for 5 s. While the use of a shorter excitation wavelength resulted in shorter response latencies than in other optogenetic

experiments, wild-type animals were similarly unresponsive in this protocol. Animals that failed to respond to the stimulus during the baseline period were excluded from the study.

Free-swimming TRPA1 stimulation (mutants and ablations)

Fish were singly placed into a 20.6 mm cut-out agarose circular mold illuminated by three quad blue LEDs (Luxeon Star, 470 nm). Following 5 min of habituation in DMSO, fish were stimulated once every 30s with a 100ms pulse of blue light. The DMSO solution was then exchanged with Optovin, and the same protocol repeated. Behavior was recorded at 200 fps (Pike F-032, Allied Vision) and analyzed using custom Python software. OXT mutant clutches were genotyped post-hoc. For nitroreductase-mediated ablations, *Tg(oxt:Gal4;UAS:nfsb-mCherry)* fish were incubated in 2.5 mM metronidazole (Sigma M-3761) from 4-6 dpf, then held in facility water until behavioral testing at 8 dpf. Ablations were confirmed by confocal imaging (Zeiss LSM800).

Statistics

All bar plots show mean ± Standard Error of the Mean (SEM) over fish. The MATLAB function notBoxPlot.m (showing mean, 1 Standard Deviation (SD) and 95% confidence interval) was used to plot data in Figures 5, 6 and S9. Significance was reported as follows: *p<0.05, **p<0.01, ***p<0.001. Significance was determined using the non-parametric Wilcoxon Signed Rank Test for paired data and the Wilcoxon Rank Sum test for independent samples. The Wilcoxon Signed Rank test was also used in Figure 1b for comparing the distribution of normalized OXT ROI signals across different behavioral stimuli to the null hypothesis of median 1. In most cases, these tests were two-sided (specified in legends). The non-parametric Kruskal-Wallis test or parametric two-way ANOVA were used when comparing fish using multiple parameters or multiple stimulation conditions. Thus, with the exception of two-way ANOVA, for which we made the assumption of normally-distributed data, nonparametric tests were used for all analyses. Bootstrapping analysis (Figure S10) was performed with custom MATLAB code by sampling with replacement individual fish, followed by individual bouts per fish, for 10000 iterations, to generate a distribution of mean differences between pre- and post-sham or M-cell ablation behavior. Pearson's correlation was used in regressor and other linear correlation analyses. No statistical methods were used to pre-determine sample sizes but our sample sizes are similar to those reported in previous publications[19,38,55]. In experiments involving *oxt−/−* mutants the researchers were blind to genotype, which was determined post-hoc. No blinding was used in any other experiment, but data was acquired and processed in a highly automated way, often by multiple independent researchers across laboratories.

Reporting Summary

Additional details for the experimental design and statistical testing used in this manuscript are available in the accompanying Life Sciences Reporting Summary.

DATA AVAILABILITY

All data, code (hardware control and analysis) and resources (transgenic lines/mutants generated) will be made available by the corresponding author upon request.

CODE AVAILABILITY

Live versions of the analysis code are maintained at www.github.com/carolinewee.

Supplementary Material

Refer to Web version on PubMed Central for supplementary material.

ACKNOWLEDGEMENTS:

We thank E. Glasgow (Georgetown University) for kindly providing the *Tg(oxt:GFP)* transgenic line and oxt:GFP plasmid, which we used to generate the oxt:Gal4 line, L. O'Connell and H. Gainer (NINDS) for providing an oxytocin antibody and M. Manning (U. Toledo) for providing us with pharmacological tools for preliminary experiments. We are especially grateful to D. Schoppik, M. Haesemeyer, D. Guggiana-Nilo and J. Yang for helping with preliminary experiments, and R. Portugues for sharing software. We also thank C-T. Yang and M. Ahrens for sharing transgenic lines used in preliminary experiments, and the Zebrafish International Resource Center (ZIRC) for providing us with the *Tg(UAS:nfsb-mCherry)* transgenic line. Support from S. Turney and the CBS imaging facility, as well as the NorthWest Undergraduate Teaching Laboratories at Harvard, were essential for the successful completion of many experiments. J. Miller, S. Zimmerman, K. Hurley and B. Hughes at Harvard, as well as the University of Utah Centralized Zebrafish Animal Resource (CZAR) provided invaluable fish care. Finally, we would like to thank N. Uchida, W. Carlezon, R. Dorsky, and C. Gregg for helpful discussions and comments. This work was supported by the Sloan Foundation (ADD), NIH grants R01-NS111067 (ADD), U01-NS090449 (FE), R24-NS086601 (FE), U19-NS104653 (FE, ADD, and SK), T32-HL007901 (AL), T32-NS076067 (SLM.), F31-NS100412-03 (JPB), DP1-HD094764 (AFS), Simons Foundation grant SCGB 325207 (FE), and NSF CAREER IOS-10043082 (ADD). CLW was supported by the National Science Scholarship from the Agency for Science, Technology and Research (A*STAR), Singapore.

REFERENCES

1. LeDoux J Rethinking the emotional brain. Neuron 73, 653–76 (2012). [PubMed: 22365542]
2. Gross CT & Canteras NS The many paths to fear. Nat. Rev. Neurosci 13, 651–8 (2012). [PubMed: 22850830]
3. Dubin AE & Patapoutian A Nociceptors: the sensors of the pain pathway. J. Clin. Invest 120, 3760–72 (2010). [PubMed: 21041958]
4. Eliava M et al. A New Population of Parvocellular Oxytocin Neurons Controlling Magnocellular Neuron Activity and Inflammatory Pain Processing. Neuron 89, 1291–304 (2016). [PubMed: 26948889]
5. Knobloch HS et al. Evoked axonal oxytocin release in the central amygdala attenuates fear response. Neuron 73, 553–66 (2012). [PubMed: 22325206]
6. Poisbeau P, Grinevich V & Charlet A in Current topics in behavioral neurosciences (2017). doi: 10.1007/7854_2017_14
7. Rojas-Piloni G et al. Oxytocin, but not vassopressin, modulates nociceptive responses in dorsal horn neurons. Neurosci. Lett 476, 32–5 (2010). [PubMed: 20371376]
8. Grillon C et al. Oxytocin increases anxiety to unpredictable threat. Mol. Psychiatry 18, 958–60 (2013). [PubMed: 23147382]
9. Striepens N et al. Oxytocin facilitates protective responses to aversive social stimuli in males. Proc. Natl. Acad. Sci. U. S. A 109, 18144–9 (2012). [PubMed: 23074247]
10. Knobloch HS & Grinevich V Evolution of oxytocin pathways in the brain of vertebrates. Front. Behav. Neurosci 8, 31 (2014). [PubMed: 24592219]

11. Wircer E et al. Homeodomain protein Otp affects developmental neuropeptide switching in oxytocin neurons associated with a long-term effect on social behavior. Elife 6, (2017).
12. Herget U, Gutierrez-Triana JA, Salazar Thula O, Knerr B & Ryu S Single-Cell Reconstruction of Oxytocinergic Neurons Reveals Separate Hypophysiotropic and Encephalotropic Subtypes in Larval Zebrafish. eneuro 4, ENEURO.0278-16.2016 (2017).
13. Coffey CM et al. Novel oxytocin gene expression in the hindbrain is induced by alcohol exposure: transgenic zebrafish enable visualization of sensitive neurons. PLoS One 8, e53991 (2013). [PubMed: 23342055]
14. Herget U, Wolf A, Wullimann MF & Ryu S Molecular neuroanatomy and chemoarchitecture of the neurosecretory preoptic-hypothalamic area in zebrafish larvae. J. Comp. Neurol 522, 1542–64 (2014). [PubMed: 24127437]
15. Swanson LW & Sawchenko PE Paraventricular nucleus: a site for the integration of neuroendocrine and autonomic mechanisms. Neuroendocrinology 31, 410–7 (1980). [PubMed: 6109264]
16. Sawchenko PE & Swanson LW Immunohistochemical identification of neurons in the paraventricular nucleus of the hypothalamus that project to the medulla or to the spinal cord in the rat. J. Comp. Neurol 205, 260–72 (1982). [PubMed: 6122696]
17. Saito D, Komatsuda M & Urano A Functional organization of preoptic vasotocin and isotocin neurons in the brain of rainbow trout: central and neurohypophysial projections of single neurons. Neuroscience 124, 973–984 (2004). [PubMed: 15026137]
18. Korn H & Faber DS The Mauthner cell half a century later: a neurobiological model for decision-making? Neuron 47, 13–28 (2005). [PubMed: 15996545]
19. Randlett O et al. Whole-brain activity mapping onto a zebrafish brain atlas. Nat. Methods 12, 1039–1046 (2015). [PubMed: 26778924]
20. Tsukamoto G & Adachi A Neural responses of rat area postrema to stimuli producing nausea. J. Auton. Nerv. Syst 49, 55–60 (1994). [PubMed: 7963265]
21. Ludwig M & Leng G Dendritic peptide release and peptide-dependent behaviours. Nat. Rev. Neurosci 7, 126–36 (2006). [PubMed: 16429122]
22. Swanson LW & Sawchenko PE Hypothalamic integration: organization of the paraventricular and supraoptic nuclei. Annu. Rev. Neurosci 6, 269–324 (1983). [PubMed: 6132586]
23. Prober DA et al. Zebrafish TRPA1 channels are required for chemosensation but not for thermosensation or mechanosensory hair cell function. J. Neurosci 28, 10102–10 (2008). [PubMed: 18829968]
24. Venkatachalam K, Luo J & Montell C Evolutionarily conserved, multitasking TRP channels: lessons from worms and flies. Handb. Exp. Pharmacol 223, 937–62 (2014). [PubMed: 24961975]
25. Bautista DM, Pellegrino M & Tsunozaki M TRPA1: A Gatekeeper for Inflammation. (2013). at <http://www.annualreviews.org/doi/abs/10.1146/annurev-physiol-030212-183811>
26. Gau P et al. The zebrafish ortholog of TRPV1 is required for heat-induced locomotion. J. Neurosci 33, 5249–60 (2013). [PubMed: 23516290]
27. Patapoutian A, Tate S & Woolf CJ Transient receptor potential channels: targeting pain at the source. Nat. Rev. Drug Discov 8, 55–68 (2009). [PubMed: 19116627]
28. Macpherson LJ et al. Noxious compounds activate TRPA1 ion channels through covalent modification of cysteines. Nature 445, 541–5 (2007). [PubMed: 17237762]
29. Kokel D et al. Photochemical activation of TRPA1 channels in neurons and animals. Nat. Chem. Biol 9, 257–63 (2013). [PubMed: 23396078]
30. Lam P-Y et al. A high-conductance chemo-optogenetic system based on the vertebrate channel Trpa1b. Sci. Rep 7, 11839 (2017). [PubMed: 28928472]
31. Orger MB & Portugues R in Methods in molecular biology (Clifton, N.J.) 1451, 307–320 (2016).
32. Guggiana-Nilo DA & Engert F Properties of the Visible Light Phototaxis and UV Avoidance Behaviors in the Larval Zebrafish. Front. Behav. Neurosci 10, 160 (2016). [PubMed: 27594828]
33. van den Pol AN Neuropeptide Transmission in Brain Circuits. Neuron 76, 98–115 (2012). [PubMed: 23040809]

34. Hrabovszky E & Liposits Z Novel aspects of glutamatergic signalling in the neuroendocrine system. J. Neuroendocrinol 20, 743–51 (2008). [PubMed: 18601697]
35. Stoop R Neuromodulation by oxytocin and vasopressin. Neuron 76, 142–59 (2012). [PubMed: 23040812]
36. Herget U & Ryu S Coexpression analysis of nine neuropeptides in the neurosecretory preoptic area of larval zebrafish. Front. Neuroanat 9, 2 (2015). [PubMed: 25729355]
37. Fetcho JR, Higashijima S & McLean DL Zebrafish and motor control over the last decade. Brain Res. Rev 57, 86–93 (2008). [PubMed: 17825423]
38. Liu KS & Fetcho JR Laser ablations reveal functional relationships of segmental hindbrain neurons in zebrafish. Neuron 23, 325–35 (1999). [PubMed: 10399938]
39. O'Malley DM, Kao YH & Fetcho JR Imaging the functional organization of zebrafish hindbrain segments during escape behaviors. Neuron 17, 1145–1155 (1996). [PubMed: 8982162]
40. Vom Berg-Maurer CM, Trivedi CA, Bollmann JH, De Marco RJ & Ryu S The Severity of Acute Stress Is Represented by Increased Synchronous Activity and Recruitment of Hypothalamic CRH Neurons. J. Neurosci 36, 3350–62 (2016). [PubMed: 26985042]
41. Gutierrez-Triana JA, Herget U, Lichtner P, Castillo-Ramírez LA & Ryu S A vertebrate-conserved cis-regulatory module for targeted expression in the main hypothalamic regulatory region for the stress response. BMC Dev. Biol 14, 41 (2014). [PubMed: 25427861]
42. Amir-Zilberstein L et al. Homeodomain protein otp and activity-dependent splicing modulate neuronal adaptation to stress. Neuron 73, 279–91 (2012). [PubMed: 22284183]
43. Wagenaar D. a, Hamilton MS, Huang T, Kristan WB & French K. a. A hormone-activated central pattern generator for courtship. Curr. Biol 20, 487–95 (2010). [PubMed: 20226670]
44. Pearson S. a, Mouihate A, Pittman QJ & Whelan PJ Peptidergic activation of locomotor pattern generators in the neonatal spinal cord. J. Neurosci 23, 10154–63 (2003). [PubMed: 14602832]
45. Dose F, Zanon P, Coslovich T & Taccola G Nanomolar oxytocin synergizes with weak electrical afferent stimulation to activate the locomotor CpG of the rat spinal cord in vitro. PLoS One 9, e92967 (2014). [PubMed: 24658101]
46. Owen SF et al. Oxytocin enhances hippocampal spike transmission by modulating fast-spiking interneurons. Nature 500, 458–462 (2013). [PubMed: 23913275]
47. Marlin BJ & Froemke RC Oxytocin modulation of neural circuits for social behavior. Dev. Neurobiol 77, 169–189 (2017). [PubMed: 27626613]
48. Guzmán YF et al. Fear-enhancing effects of septal oxytocin receptors. Nat. Neurosci 16, 1185–7 (2013). [PubMed: 23872596]
49. Nersesyan Y et al. Oxytocin Modulates Nociception as an Agonist of Pain-Sensing TRPV1. Cell Rep. 21, 1681–1691 (2017). [PubMed: 29117570]
50. Reiter MK et al. Localization of oxytocin binding sites in the thoracic and upper lumbar spinal cord of the adult and postnatal rat: a histoautoradiographic study. Eur. J. Neurosci 6, 98–104 (1994). [PubMed: 8130936]

METHODS REFERENCES:

51. Kim DH et al. Pan-neuronal calcium imaging with cellular resolution in freely swimming zebrafish. Nat. Methods (2017). doi:10.1038/nmeth.4429
52. Muto A et al. Activation of the hypothalamic feeding centre upon visual prey detection. Nat. Commun 8, 15029 (2017). [PubMed: 28425439]
53. Davison JM et al. Transactivation from Gal4-VP16 transgenic insertions for tissue-specific cell labeling and ablation in zebrafish. Dev. Biol 304, 811–24 (2007). [PubMed: 17335798]
54. Miyasaka N et al. From the olfactory bulb to higher brain centers: genetic visualization of secondary olfactory pathways in zebrafish. J. Neurosci 29, 4756–67 (2009). [PubMed: 19369545]
55. Lacoste AMB et al. A convergent and essential interneuron pathway for Mauthner-cell-mediated escapes. Curr. Biol 25, 1526–34 (2015). [PubMed: 25959971]
56. Scott EK et al. Targeting neural circuitry in zebrafish using GAL4 enhancer trapping. Nat. Methods 4, 323–6 (2007). [PubMed: 17369834]

57. Ben Fredj N et al. Synaptic activity and activity-dependent competition regulates axon arbor maturation, growth arrest, and territory in the retinotectal projection. J. Neurosci 30, 10939–51 (2010). [PubMed: 20702722]

58. Montague TG, Cruz JM, Gagnon JA, Church GM & Valen E CHOPCHOP: a CRISPR/Cas9 and TALEN web tool for genome editing. Nucleic Acids Res. 42, W401–7 (2014). [PubMed: 24861617]

59. Gagnon JA et al. Efficient mutagenesis by Cas9 protein-mediated oligonucleotide insertion and large-scale assessment of single-guide RNAs. PLoS One 9, e98186 (2014). [PubMed: 24873830]

60. Schindelin J et al. Fiji: an open-source platform for biological-image analysis. Nat. Methods 9, 676–682 (2012). [PubMed: 22743772]

61. Altstein M & Gainer H Differential biosynthesis and posttranslational processing of vasopressin and oxytocin in rat brain during embryonic and postnatal development. J. Neurosci 8, 3967–77 (1988). [PubMed: 3183709]

62. Thisse C & Thisse B High-resolution in situ hybridization to whole-mount zebrafish embryos. Nat. Protoc 3, 59–69 (2008). [PubMed: 18193022]

63. Thevenaz P, Ruttimann UE & Unser M A pyramid approach to subpixel registration based on intensity. IEEE Trans. Image Process. 7, 27–41 (1998). [PubMed: 18267377]

64. Chen T-W et al. Ultrasensitive fluorescent proteins for imaging neuronal activity. Nature 499, 295–300 (2013). [PubMed: 23868258]

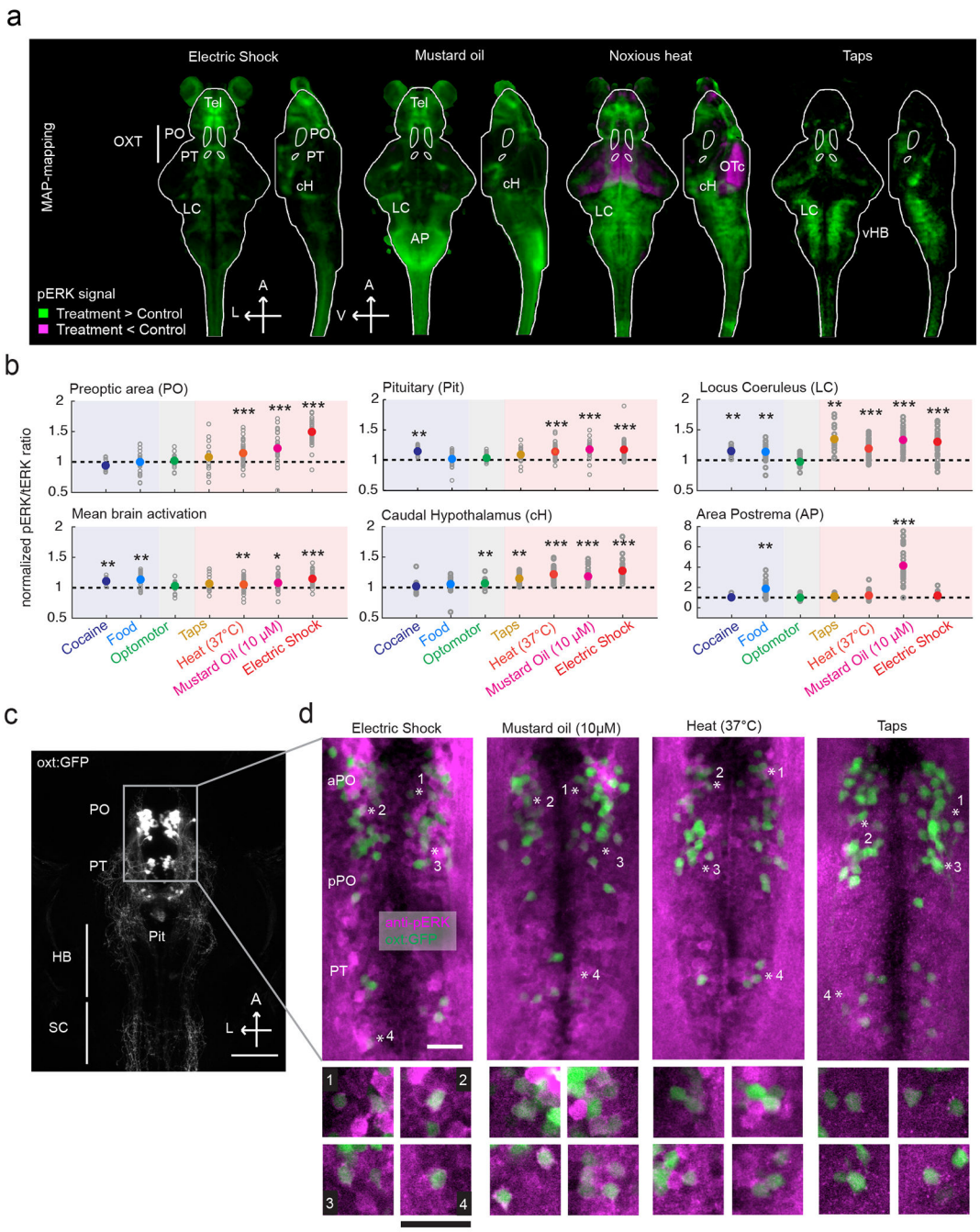

Figure 1: Brain-wide responses to noxious and aversive stimuli

(a) Whole-brain MAP-mapping experiments showing neural responses to a range of aversive stimuli. Each map was generated by pooling and analyzing data across multiple experiments to generate a composite map. Maps display voxels that are significantly activated (green) or inhibited (magenta) across multiple experiments, by electric shock (three experiments), mustard oil (two 10 μM and one 25 μM experiment), 37°C heat (three experiments) and dish taps (two experiments). The brain is outlined in white. Mustard oil treatment also induced pERK expression outside of the brain, especially in skin and muscle tissue. These data

include the single experiments previously published in Randlett et al. (2015), combined with new experiments. Scale bar = 100 μm. PO = preoptic area (white outline), PT = posterior tuberculum (white outline), LC = Locus coeruleus, cH = caudal hypothalamus, AP = Area Postrema, vHB = ventral hindbrain, OTc = Optic Tectum. A = anterior, L = Left, V = Ventral.

(b) Comparison of PO (top leftmost) and whole brain (bottom leftmost) activation in response to a range of appetitive (cocaine, food), neutral (optomotor gratings) and aversive (dish taps, 37°C heat, mustard oil, electric shock) stimuli. Background shading represents stimulus valence (blue = positive, red = negative, gray = neutral). Fold change in PO vs. whole brain activity: 0.94±0.03 / 1.1±0.01 (cocaine); 1.00±0.04 / 1.13±0.02 (food); 1.02±0.02 / 1.02±0.02 (OMR); 1.08±0.08 / 1.06±0.04 (taps); 1.14±0.02 / 1.04±0.01 (heat); 1.22±0.04 / 1.08±0.02 (mustard oil); 1.49±0.03 / 1.14±0.02 (electric shock).
Adjusted p-values for these ratios are 0.19 / **0.003 (cocaine); 6.19 / **0.002 (food); 2.11 / 0.36 (OMR); 2.90 / 1.51 (taps); ***$4.77x10^{-6}$ / **0.008 (heat); ***$2.13x10^{-4}$ / *0.012 (10 μM mustard oil); ***$4.30\ x10^{-7}$ / ***$1.70x10^{-6}$ (electric shock). n = 12/22/23/13/50/32/39 fish pooled across multiple experiments, two-sided Wilcoxon Signed Rank test against median of 1, Bonferroni Correction. Also shown are examples of other brain regions that were affected by aversive or noxious stimuli. The pituitary (hypophysis) showed significant enhancement in pERK signals for electric shock (1.17 fold, ***$p = 5.03x10^{-7}$), 10 μM mustard oil (1.18 fold, ***$p = 6x10^{-5}$), heat (1.14 fold, ***$p = 1.86x10^{-8}$), and cocaine (1.16 fold, **p = 0.0034). The norepinephrinergic locus coeruleus (LC) showed strong activation by taps (1.34 fold, **p=0.0017), mustard oil (1.32 fold, ***$p = 5.57x10^{-6}$) and electric shock (1.30 fold, ***$p = 8.98x10^{-6}$), and slightly weaker activation by heat (1.18 fold, ***$p = 4.73x10^{-8}$), cocaine (1.14 fold, **p = 0.0034) and food (1.13 fold, **p = 0.0097). The caudal hypothalamus (cH) was significantly activated by electric shock (1.27 fold, $p = 3.68x10^{-7}$), mustard oil (1.18 fold, $p = 5.57x10^{-6}$), heat (1.21 fold, $p = 5.29x10^{-9}$), taps (1.14 fold, **p = 0.0017), and more weakly by optomotor stimuli (1.06 fold, **p=0.0014). The area postrema (AP) was highly activated by mustard oil (4.12 fold, ***$p = 6.13x10^{-6}$, note change in y-scale) and relatively weakly by electric shock (1.17 fold, ***$p = 3.22x10^{-4}$). It is also strongly activated by food stimuli (1.85 fold, **p = 0.0011).

(c) Z-projection image of *Tg(oxt:GFP)* fish showing OXT neurons in the PO and PT, and their projections to the pituitary gland (Pit), hindbrain (HB) and spinal cord (SC), among other regions. Scale bar = 100 μm.

(d) Top: Z-projection image of dissected brain showing overlap of oxt:GFP-positive (green) neurons with pERK staining after 15 min of electric shock (30s inter-stimulus interval (ISI), 100 ms shock, 6V/cm, representative image of 2 datasets), mustard oil treatment (10 μM, representative image of 3 datasets), noxious heat (37°C, representative image of 3 datasets), and taps (30s ISI, representative image of 2 datasets). Results from these datasets are further analyzed in Figure 2. Scale bar = 20 μm. Both OXT and surrounding non-OXT neurons were activated by these stimuli. Bottom (inset): Examples of putative overlap between OXT expression and pERK staining corresponding to regions indicated by numbered asterisks. Black scale bar (box width) = 20 μm. White scale bar = 20 μm. aPO/pPO = anterior/ posterior preoptic area.

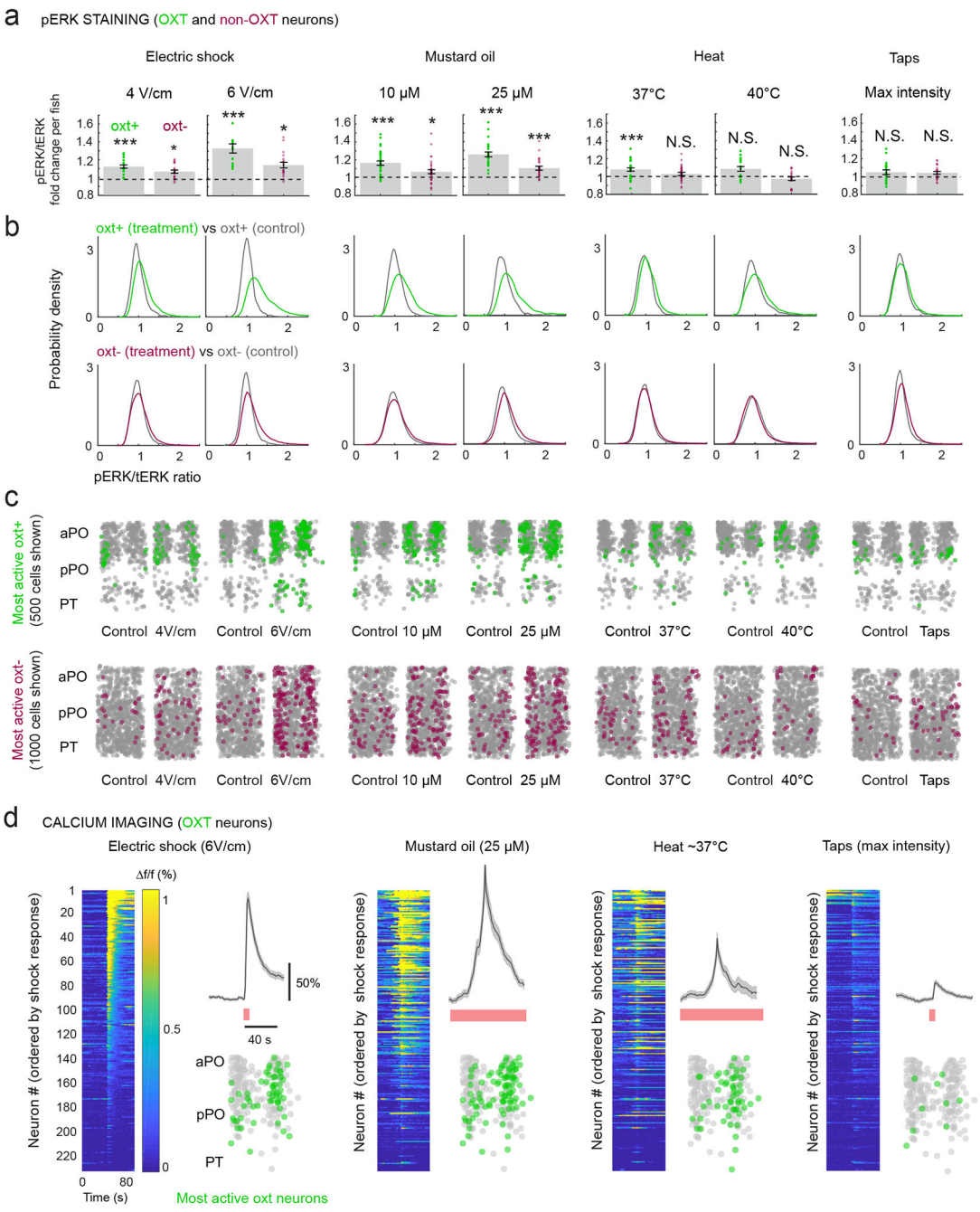

Figure 2: Cellular analysis of OXT activity reveals preferential activation by noxious stimuli

(a) Fold change in mean OXT (green) and neighboring non-OXT (purple) neuron pERK activity by fish, relative to controls. Data shown in this figure are from high-resolution images acquired from dissected brains. pERK/tERK ratios of individual *Tg(oxt:GFP)*-positive neurons were normalized to the mean pERK/tERK ratios of OXT neurons in control fish within each experiment, and aggregated over multiple experiments. Shock 4V/cm: ***p = 6.16×10^{-5}, fold increase = 1.12 (OXT), *p = 0.02, fold increase = 1.06 (non-OXT), n = 14 control/20 treatment; Shock 6V/cm: ***p = 8.06×10^{-7}, fold increase = 1.34 (OXT), ***p =

$2.63x10^{-4}$, fold increase = 1.15 (non-OXT), n = 19 control/19 treatment; 10 μM MO: ***p = $1.42x10^{-6}$, fold increase = 1.17 (OXT), *p = 0.0381, fold increase = 1.06 (non-OXT), n = 33 control/35 treatment; 25 μM MO: ***p = $6.87x10^{-9}$, fold increase = 1.26 (OXT), ***p = $3.08x10^{-4}$, fold increase = 1.11 (non-OXT), n = 25 control /26 treatment; 37°C Heat: ***p = $5.40x10^{-4}$, fold increase = 1.08 (OXT), p = 0.14, fold increase = 1.03 (non-OXT), n= 38 control/32 treatment, 40°C Heat: p = 0.06, fold increase = 1.09 (OXT), p = 0.4, fold increase = 0.97 (non-OXT), n = 12 control/19 treatment, Taps: p = 0.12, mean increase = 1.05 (OXT), p = 0.09, mean increase =1.05 (non-OXT), n = 22 control/22 treatment, two-sided Wilcoxon Rank Sum test.

(b) Probability distributions (kernel density estimate (KDE)) of pERK/tERK ratios for individual OXT (green, top) and non-OXT (purple, bottom) neurons after treatment with noxious/aversive stimuli, as compared to control distributions (gray). Electric shock and mustard oil induced the strongest right-shift in pERK/tERK ratios, with OXT neurons showing a larger increase than non-OXT neurons.

(c) Spatial distribution of the most strongly activated OXT (top, green) and non-OXT (bottom, purple) neurons in the PO and PT. To be classified as highly active, pERK/tERK ratios must exceed the threshold at which <3% of OXT neurons in control conditions would be considered active. The same threshold is applied to non-OXT neurons. To account for differences in neuron number due to varying dataset sizes, 500 randomly-sampled OXT neurons, and 1000 randomly-sampled non-OXT neurons are displayed per experimental group.

(d) Calcium imaging of OXT neurons in response to noxious stimuli. The same fish (n = 231 neurons from 7 independent fish) were exposed to electric shock (6V/cm), mustard oil (25 μM, bath exposure), heat (peak temperature >37°C) and taps (suprathreshold to elicit startle behavior). Raster plots show average calcium responses of all neurons tested, sorted by the strength of their shock responses. Neuron number is consistent across all raster plots, allowing for comparison across stimuli. Shock and tap responses were aligned using the onset of the stimulus, while mustard oil and heat signals were aligned to the maximum response within 60 s of stimulus delivery. Calcium traces show the average response across all neurons, shading indicates SEM. Red bar indicates stimulus period. In order to quantify the spatial distribution of activated neurons, we set a threshold (integrated calcium signal =1, See Figure S3) above which neurons were considered to be highly active. This method likely underestimates the extent of activation by these stimuli, since weakly activated neurons (e.g. from tap stimuli) would be excluded.

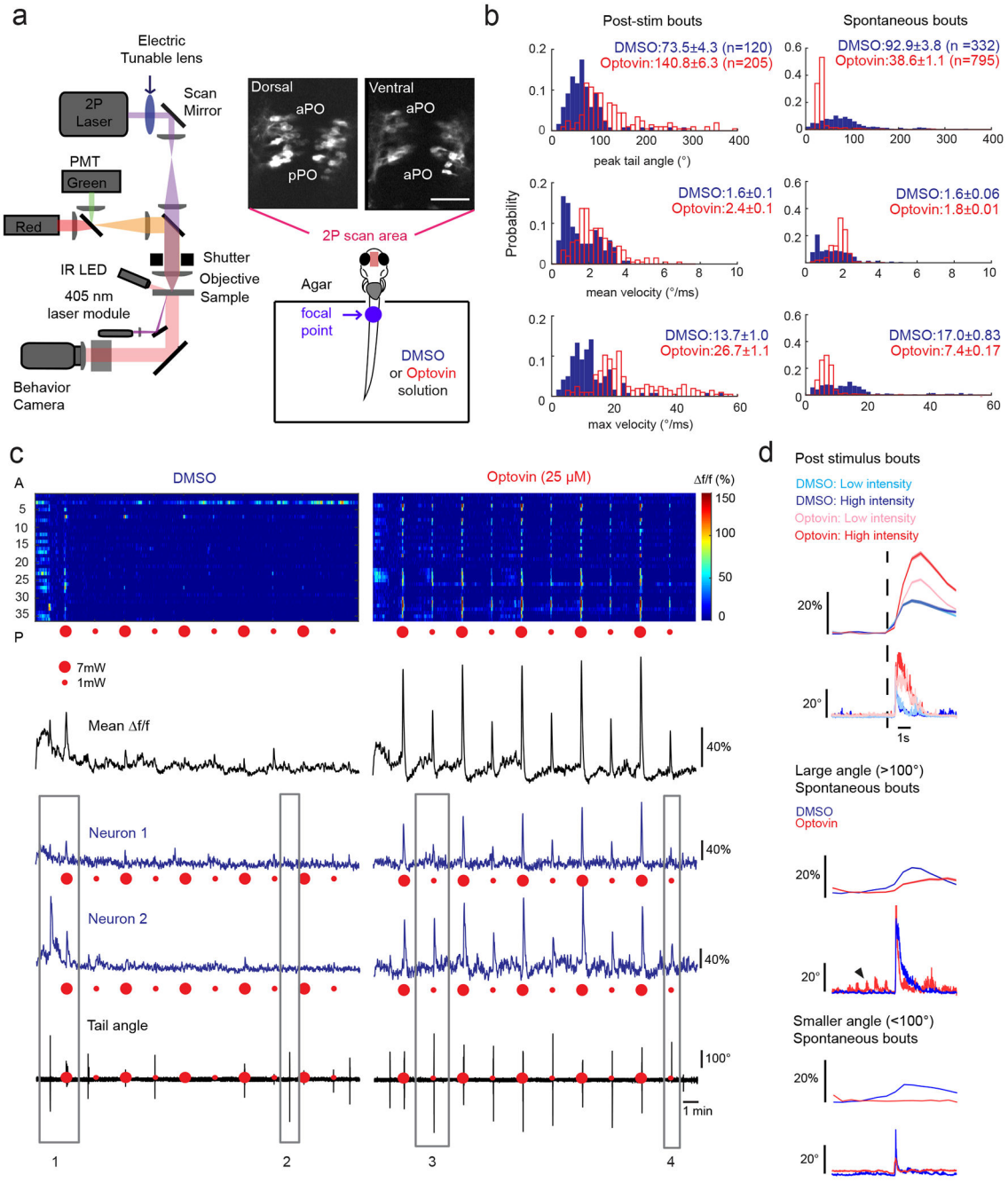

Figure 3: OXT neuron activity correlates with TRPA1 stimulus and avoidance behavior

(a) Schematic of TRPA1 stimulation setup for volumetric calcium imaging. An electrically-tunable lens was used for volumetric imaging of the OXT population, labeled by *Tg(oxt:Gal4;UAS:GCaMP6s)*. 2-3 z volumes were sufficient to span the entire population. Images show ventral and dorsal views in a representative fish. Scale bar = 50 µm. Fish were stimulated using a 405 nm laser focused on the bottom of the anterior part of the tail.

(b) Probability distribution of peak tail angles, maximum and mean swim velocity of extracted bouts that occurred either post-stimulus (i.e. within 5 s of stimulus) or

spontaneously (all other times). UV stimulation in Optovin (i.e. TRPA1 stimulation) significantly increased the number of bouts (n_{bouts}= 120/205 (DMSO/Optovin), tail angle magnitude (***$1.8x10^{-21}$), mean tail velocity (***p = $8.2x10^{-10}$) and maximum tail velocity (***$6.6x10^{-25}$) in Optovin (red) compared to DMSO (blue). While spontaneous swim frequency (n_{bouts} = 332/795 (DMSO/Optovin) was also increased in Optovin, there was a significant reduction in peak angle magnitude (***p = $6.5x10^{-69}$), and maximum velocity (***p = $1.3x10^{-46}$) during spontaneous events, and a small increase in mean velocity (***p = $4.1x10^{-16}$), when bouts were pooled across fish (two-sided Wilcoxon Rank Sum test). Statistics by fish (post-stimulus): ***p = $4.9x10^{-4}$ (frequency) / ***$2.4x10^{-4}$(peak angle) / ***$2.4x10^{-4}$(max velocity) / ***$4.9x10^{-4}$ (mean velocity). Statistics by fish (non-stimulus bouts): p = 0.35 (frequency) / 0.052 (peak angle) / 0.57 (mean velocity) / ***$4.9x10^{-4}$ (max velocity *decrease*) n = 14 fish, two-sided Wilcoxon Signed Rank test.

(c) Volumetric imaging of an example *Tg(oxt:Gal4;UAS:GCaMP6s)* fish. Raster plots show Δf/f activity traces for all visible OXT neurons (n=38 neurons, 2 non-overlapping z-planes) for the entire experiment (10 UV stimuli of 100 ms duration alternating between 2 intensities (1mW and 7mW), 120 s inter-stimulus interval (ISI)). In this plot, neurons are sorted along the A-P axis. The same neurons were visually identified in both the DMSO and Optovin conditions. Bottom: Average Δf/f for all neurons and simultaneously recorded tail angle traces. Red dots represent UV stimuli, with larger dots representing the higher intensity stimulus. Two example neurons are shown -- Neuron 1 appears strongly correlated with the TRPA1 stimulus and Neuron 2 shows activity more consistent with behavioral correlation. Four gray boxes provide examples of: 1) Spontaneous and post-UV stimulus activation of Neuron 2 that correlates with motor output; 2) Spontaneous large-angle motor output that is not reflected by activity of either neuron; 3) Large-angle tail bend that occurs during weak TRPA1 (Optovin + UV) stimulus, with Neuron 1 showing weak activation, and Neuron 2 showing strong activation; 4) Weak behavioral output corresponding to weak TRPA1 stimulus, where both Neurons 1 and 2 similarly show weak activation.

(d) Bout-triggered averages of calcium activity (Δf/f) and tail angle (°) in DMSO and Optovin for either the first bouts post-stimulation (1mW and 7mW light intensity; top panels, n = 2516 (DMSO; 1mW), 3312 (Optovin; 1mW), 2123 (DMSO; 7mW), 2648 (Optovin; 7mW) calcium traces corresponding to 61, 84, 53, and 67 detected bouts from 14 fish), spontaneous bouts with peak tail angle magnitude above 100° (middle panels, n = 3959 (DMSO) and 1460 (Optovin) calcium traces corresponding to 103 and 34 detected bouts from 14 fish), or spontaneous bouts with peak tail angle magnitude below 100° (bottom panels n = 9595 (DMSO) and 26112 (Optovin) calcium traces corresponding to 229 and 761 detected bouts from 14 fish). Black arrow identifies small-amplitude tail twitches that occasionally occur in the Optovin condition after repeated UV stimulation. These twitches are usually indistinguishable from noise and did not affect correlational analyses.

(e) Scale bars represent either 20% Δf/f or 20° tail angle for calcium and tail angle traces respectively. Shading for calcium traces (where visible) represents S.E.M. Since the peak tail angle magnitudes per bout were measured within a 5 s window from bout onset, the average peak magnitude may not correspond to the peak magnitude of individual bouts.

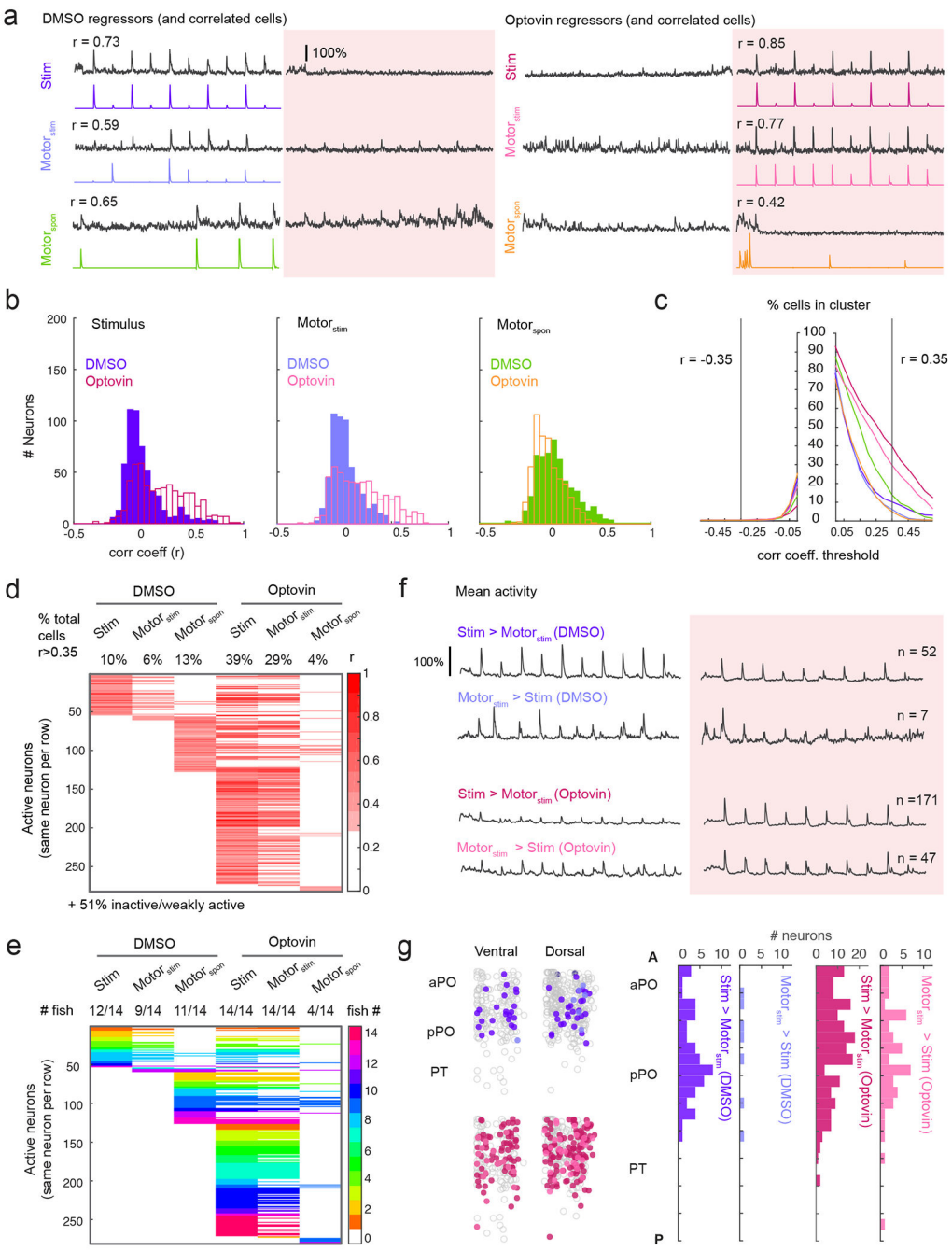

Figure 4: Diversity of sensorimotor encoding by OXT neurons

(a) Regressors for 6 neuron classes, corrresponding to the stimulus, stimulus-locked behavior ($motor_{stim}$) and spontaneous ($motor_{spon}$) behavior in both DMSO and Optovin, and Δf/f traces from an example neuron that shows strong correlation with each regressor. The neuron's response in DMSO and Optovin (shaded pink area) are shown. Note that each neuron may correlate with more than one regressor.

(b) Histograms showing Pearson correlation coefficients (r-values) of all neurons to all 6 regressors. Many neurons show high correlation to the stimulus and $motor_{stim}$ regressors in

Optovin than in DMSO (i.e. TRPA1 responsive neurons). Mean $increase_{stim}$ = 0.17, p = $8.15x10^{-41}$; mean $increase_{motorstim}$ = 0.13, p = $1.29x10^{-23}$; mean $increase_{motorspon}$ = −0.07, p = $8.82x10^{-15}$, one-sided Wilcoxon Rank Sum test.

(c) The percentage of cells that would be classified into each cluster as a function of the cutoff r-value used. At all thresholds, the largest clusters would correspond to neurons showing high correlation to the stimulus and $motor_{stim}$ regressors in Optovin (i.e. TRPA1 responsive neurons). Colors correspond to neuronal subtypes shown in (a) and (b). We set our cutoff at a stringent threshold of r = 0.35 (see Figure S4b).

(d) Classification of neurons into 6 different response types. Each row corresponds to a single neuron, and the correlation coefficients to the corresponding regressors are represented by color intensity. 49% of neurons belong to at least one of the clusters. Neurons that belong to none of the clusters (“inactive/weakly active neurons”, 279/552 neurons, 51%) are not shown. Numbers shown above each column correspond to the percentage of neurons belonging to each category.

(e) Clustered neurons color-coded by individual fish highlights both similarities across fish (e.g. Optovin stimulus and $motor_{stim}$-correlated neurons) as well as individual variability. Numbers shown above correspond to the fraction of all fish in which neurons belonging to each category were identified. All fish had stimulus- and motor-correlated neurons in Optovin trials. However, not all fish tested had stimulus or $motor_{stim}$-correlated neurons in DMSO.

(f) Mean calcium activity of neurons with either higher or lower stimulus (versus motor) correlations in DMSO or Optovin. Given that stim and $motor_{stim}$ regressors are themselves correlated, many of these neurons in fact are correlated with both regressors. However, strongly stimulus-correlated neurons show higher intensity tuning, whereas strongly motor-correlated neurons have more varied activity patterns due to variation in motor behavior.

(g) Left: 2D spatial distribution of neuronal classes described in **(f)**; Right: histogram of neurons from each class found at each position along the anterior-posterior axis. For visualization purposes, the scale (i.e. number of neurons) for Optovin stimulus-correlated neurons is different from other groups. Highly motor-correlated neurons tend to be concentrated more posteriorly.

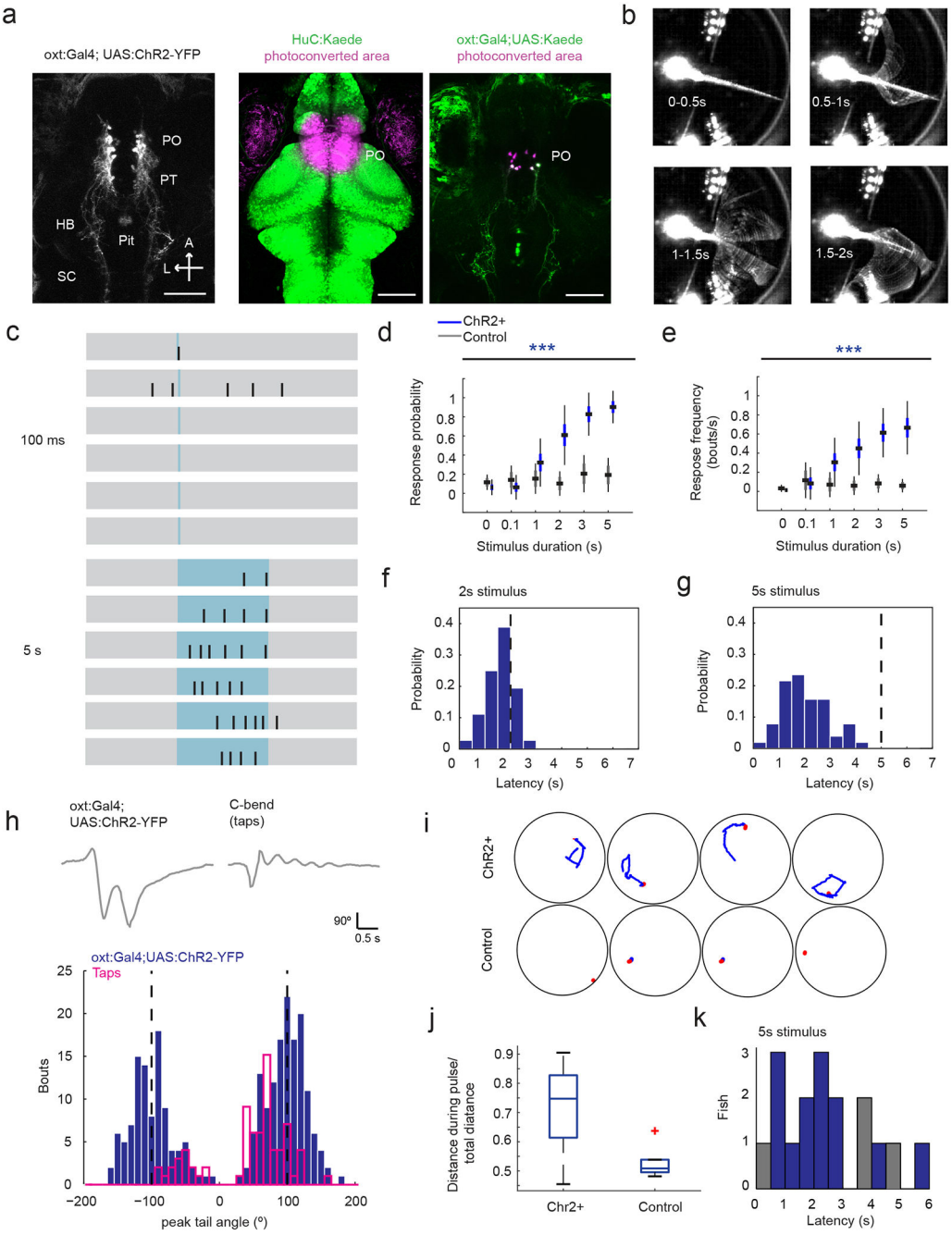

Figure 5: Optogenetic activation of OXT neurons drives large-angle tail bends

(a) Maximum intensity projection of *Tg(oxt:Gal4;UAS:ChR2-YFP)* fish shows strong PO expression and projections to the pituitary (Pit), hindbrain (HB) and spinal cord (SC) (left). Photo-conversion of *Tg(HuC:Kaede)* (center), and *Tg(oxt:Gal4;UAS:Kaede)* (right) fish marks the region that is exposed to light during optogenetic stimulation. Scale bar = 100 μm. These experiments were repeated on 3 fish each with similar results.

(b) Maximum intensity projection images showing behavior of a representative *Tg(oxt:Gal4;UAS:ChR2-YFP)* fish during different time periods after blue light onset. These experiments were repeated on more than 50 fish with similar results.
(c) Responses of a single fish to 100 ms and 5 s stimuli showing variability in response frequency and latency. Each vertical black line represents a detected swim bout. Stimulation period is highlighted in blue. Only the first 100ms stimulus produced a response. These experiments were repeated on more than 50 fish with similar results.
(d) Response probability of *Tg(oxt:Gal4;UAS:ChR2-YFP)* fish (blue) increases with stimulus duration and is significantly higher than for controls lacking ChR2-YFP expression ($F_{(1, 240)}$ = 139.48, ***p = $1.12x10^{-25}$, n = 29/13, two-way ANOVA). There was a significant interaction between genotypes and stimulus duration (*** p = $1.38x10^{-22}$). Data were pooled over multiple clutches. A single pulse of the stipulated duration was delivered for each 30 s trial. Center black line = Mean, Box = 1 SD, range = 95% confidence interval.
(e) Normalized response frequency for the same group of fish increases with stimulus duration and is significantly higher than for controls ($F_{(1, 240)}$ = 106.81, ***p=$5.99x10^{-21}$, n = 29/13, two-way ANOVA). There was a significant interaction between genotypes and stimulus duration (*** p = $8.56x10^{-14}$). Center black line = Mean, Box = 1 SD, range = 95% confidence interval.
(f) Histogram of response latencies in head-embedded fish for a 2 s light stimulus (mean latency = 1.37 ± 0.08s, n = 36 responses from 10 fish). Dashed black lines indicate the end of blue light stimulation. Data are from a single clutch.
(g) Histogram of response latencies in the same group of head-embedded fish for a 5 s light stimulus (mean latency = 1.80 ± 0.13 s, n = 51 responses from 10 fish).
(h) Top: Example of tail bend kinematics (cumulative angle vs. time) elicited by *Tg(oxt:Gal4;UAS:ChR2-YFP)* stimulation (left), compared to a typical escape response elicited by a strong vibrational-acoustic tap stimulus (right). Bottom: Peak tail angles per bout elicited by photoactivation of OXT neurons (blue) versus a strong vibrational-acoustic tap stimulus in a different group of fish (magenta). The mean tail angle is significantly larger for *Tg(oxt:Gal4;UAS:ChR2-YFP)* stimulation (100.11 ± 1.93°, n=246 bouts from 10 fish, 5 s stimulus) than for taps (68.96 ± 3.09°, n = 75 bouts from 10 fish, ***p = $2.06x10^{-9}$, two-sided Wilcoxon Rank Sum test). Dashed black lines indicate 100°, which is the mean peak tail angle from *Tg(oxt:Gal4;UAS:ChR2-YFP)* stimulation.
(i) ChR2-driven free-swimming behavior in blind fish. Example swim trajectories from representative ChR2-positive fish and controls. Red = pre-pulse swim trajectory, Blue = post-pulse swim trajectory.
(j) ChR2-positive fish showed a significant increase in distance traveled during the light pulse (normalized to total distance traveled). ChR2: 0.716 ± 0.037, Controls: 0.53 ± 0.02, n = 14/6, *p = 0.015, two-sided Wilcoxon Rank Sum test. Box plot shows median, interquartile range and entire data range excluding outliers. Outliers depicted by red crosses.
(k) Histogram of mean latencies per fish for ChR2-positive (blue, 2.36 ± 0.41 s) and control (gray, 3.2 ± 0.79 s) fish. Since many control fish did not swim at all, fewer data points are depicted for that group.

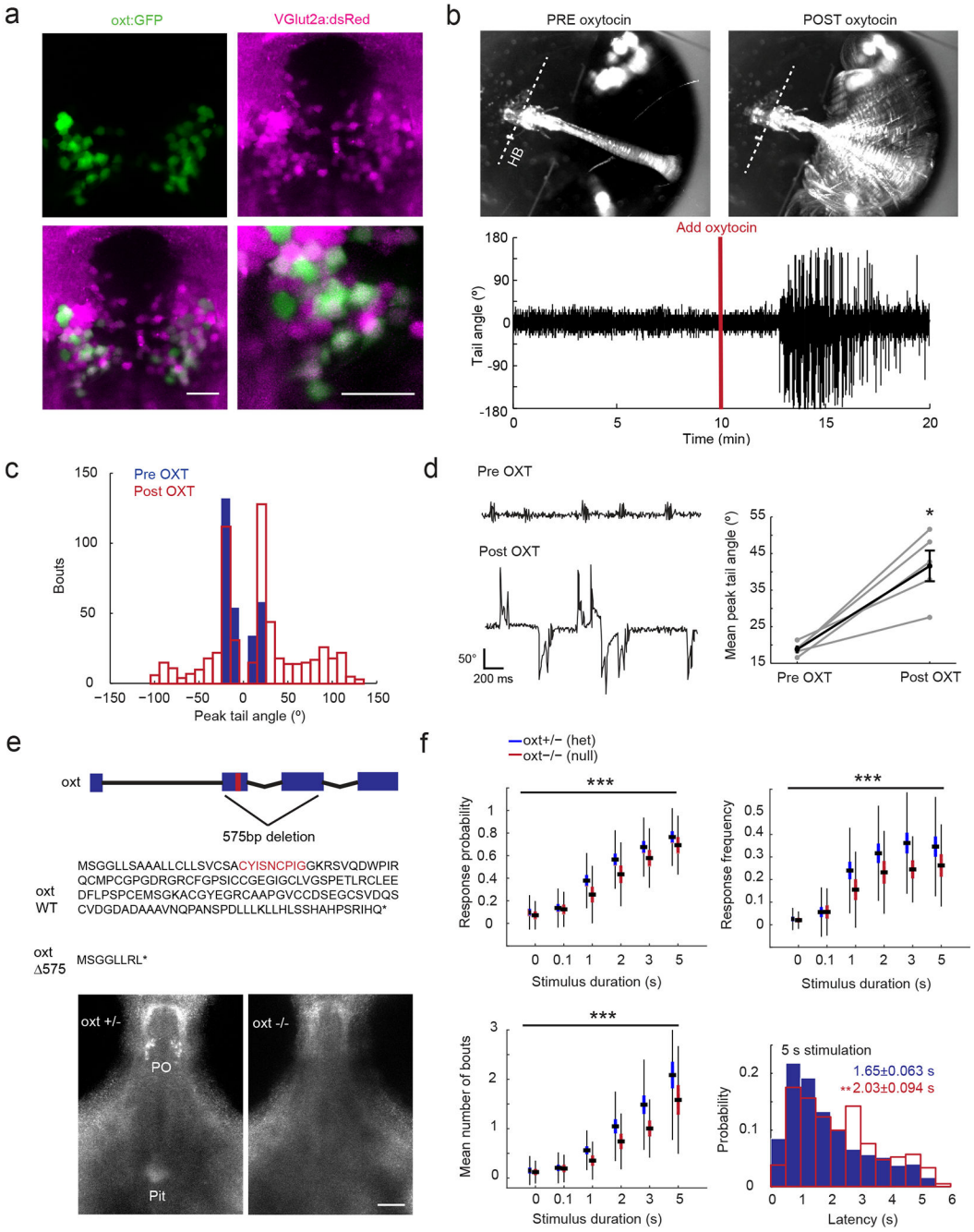

Figure 6: Role of OXT neuropeptide in driving large-angle tail bends

(a) Maximum intensity projections show *Tg(oxt:GFP)* neurons (green) overlapping with glutamate-expressing neurons labeled by *Tg(VGlut2a:dsRed)* (magenta). Bottom-right image shows a higher magnification view. Scale bar = 20 μm. The experiment was repeated on 8 fish with similar results.

(b) Top: Maximum intensity projection images of a tethered fish in a reduced preparation from a 5 min interval before and after the addition of 5 μM OXT. HB = hindbrain; more

anterior tissue was removed. Bottom: Example trace showing tail angle vs. time in this reduced preparation. The experiment was repeated on 5 fish with similar results.

(c) Distribution of peak tail angles per bout for a 10 min period before (blue) and after (red) addition of OXT, for the fish shown in (b). Peak tail angles are significantly higher after addition of OXT. Before: 16.57 ± 0.17°, n = 278 detected bouts; After: 42.49 ± 1.31°, n = 576 detected bouts, ***p = $2.27x10^{-61}$, two-sided Wilcoxon Rank Sum test.

(d) Left: Representative tail angle traces showing pre- and post-OXT behavior. Right: Peak tail angles are higher in the 10 min after addition of OXT than in the 10 min prior (*p=0.0312, n=5 fish, one-sided Wilcoxon Signed Rank test).

(e) Top: Schematic showing the zebrafish OXT gene. Exons 2 and 3, which include the sequence coding for the OXT peptide (red), are deleted in the *oxt* mutants. Predicted amino acid sequences for the products of the WT *oxt* gene and the *oxt* mutant allele are shown at bottom, with mutated amino acids in bold. Bottom images: Antibody staining against OXT confirms the absence of the peptide in homozygous *oxt−/−* (null) mutants. Scale bar = 50 μm. Faint neuropil visible in *oxt−/−* fish is due to background staining. The experiment was repeated on 4 heterozygous and 3 null mutants with similar results.

(f) Response probability, frequency and the number of responses per optogenetic stimulus are reduced in *oxt−/−* mutants. Data shown are aggregated over multiple clutches of fish. Examples of data from individual clutches are shown in Figure S9. Difference in response probability: $F_{(1, 846)} = 21.98$, ***p = $3.22x10^{-6}$, normalized frequency: $F_{(1, 846)} = 26.90$, ***p = $2.68x10^{-7}$, number of bouts: $F_{(1, 846)} = 26.49$, ***p = $3.30x10^{-7}$, n = 92 heterozygous and 51 null fish, two-way ANOVA. For response frequency, there is a significant interaction between genotype and stimulus duration (*p = 0.0207). Center black line = mean, Box = 1 SD, range = 95% confidence interval. Bottom right: Response latencies during a 5 s stimulus are significantly longer for null mutants (mean= 2.03 ± 0.094 s) than for their heterozygous (mean = 1.65 ± 0.063 s) siblings. **Adjusted p = 0.0013, n = 422/212 bouts, two-sided Wilcoxon Rank Sum test, Bonferroni correction.

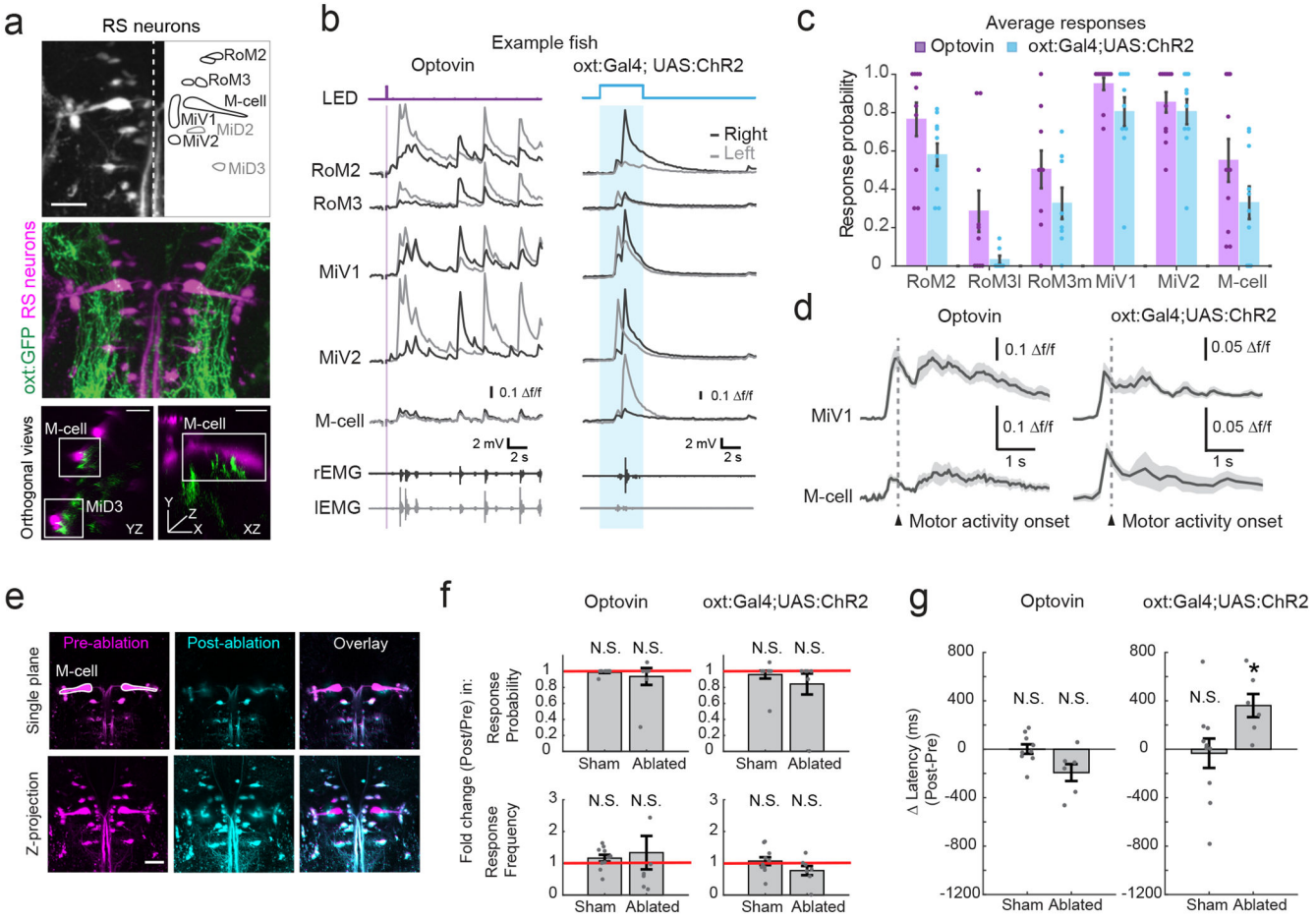

Figure 7: TRPA1 and OXT activation drive brainstem reticulospinal neurons

(a) Axons of OXT neurons (green) project to the hindbrain and co-localize with reticulospinal (RS) neurons (magenta). The RS cell types where activity was measured are highlighted in the top panel (black). MiD2 and MiD3 (gray) are M-cell homologs that also respond to Optovin and ChR2 stimulation, but were not consistently labeled by backfilling and hence excluded from analysis. Bottom panel: Orthogonal views of OXT axon proximity to RS cell types, including the M-cell. Scale bars = 20 μm. The experiment was repeated on 12 fish with similar results.

(b) Example traces showing calcium activity evoked in reticulospinal neurons by TRPA1 stimulation (Optovin, left panel) or optogenetic activation of oxytocin neurons (*Tg(oxt:Gal4;UAS:ChR2-YFP)*, right panel), along with simultaneous EMG recordings. Pulses of UV (410 nm, 100 ms) or blue (480 nm, 5 s) light were used to activate Optovin and ChR2 respectively. Black traces represent neuronal and EMG activity from the right side of the fish and gray traces represent activity from the left. The Optovin and ChR2 experiments were repeated on 6 and 5 fish, respectively, with similar results.

(c) Response probabilities of reticulospinal neurons during Optovin stimulation (purple) or ChR2-mediated oxytocin neuron activation (blue). 5% Δf/f increase is set as the threshold for activation. Bar plots show mean ± SEM. Sample sizes for the Optovin experiment [cell number/fish number]: RoM2 [10/6], RoM3l [10/6], RoM3m [10/6], MiV1 [10/6], MiV2

[11/6], M=cell [10/6]. For the ChR2 experiment [cell number/fish number]: RoM2 [10/5], RoM3l [7/4], RoM3m [8/4], MiV1 [10/5], MiV2 [10/5], M=cell [10/5]. There is no significant difference between the two groups for any cell type (RoM2, p = 0.08; RoM3l, p = 0.10; RoM3m, p = 0.26; MiV1, p = 0.08; MiV2, p = 0.61; M-cell, p = 0.18; two-sided Wilcoxon Rank Sum test).

(d) Calcium responses of MiV1 and the M-cell aligned to the onset of the first swim bout after Optovin stimulation or ChR2-mediated OXT neuron activation (mean ± SEM). Sample size for the Optovin experiment [trial number/cell number]: MiV1 [10/1], M-cell [10/1]; for the ChR2 experiment [trial number/cell number]: MiV1 [10/1], M-cell [6/2]). Shading indicates SEM.

(e) M-cell fluorescence from an example fish pre- and post-bilateral ablation. Top: Single plane, Bottom: Maximum intensity projection. Scale bar = 20 μm. The experiment was repeated on 14 fish with similar results.

(f) Fold change in probability (top) and frequency (bottom) of response in sham controls and M-cell ablated fish, for both Optovin-mediated TRPA1 stimulation (left; n=10 fish (sham) and 7 fish (ablated), two-sided Wilcoxon Signed Rank test) and optogenetic OXT activation (right; n = 10 fish (sham) and 7 fish (ablated)). The response probabilties and frequencies were unchanged in most animals, except for some outliers (Optovin (sham, ablated): $p_{probability}$= 1, 1; $p_{frequency}$= 0.27, 0.69; ChR2 (sham, ablated): $p_{probability}$ =1, 0.5; $p_{frequency}$ = 0.87, 0.22. Two-sided Wilcoxon Signed Rank test comparing post to pre-ablation values per fish). Bar plots show mean ± SEM. Fish which had a baseline response probability of <0.5 were subsequently excluded from kinematic analysis.

(g) Mean difference in latency of response (ms) of sham controls and M-cell ablated fish. When quantified across fish, there was a non-significant reduction in response latencies for TRPA1 stimulation (left; mean increase = +1.5 ± 41.5 ms (sham), −192.7 ± 76.5 ms (ablated), n = 9/6 (sham/ablated), p = 0.91/0.06 (sham/ablated)) and a significant post-ablation increase in response latencies for optogenetic OXT activation (right; mean increase = −33.1 ± 127.9 ms (sham), +360.9 ± 104.7 ms (ablated), n = 10, 6 (sham, ablated), p = 0.85, *0.03 (sham, ablated), two-sided Wilcoxon Signed Rank test comparing post to pre-ablation latencies per fish). Bar plots show mean ± SEM. See also Figure S10 for additional measured kinematic parameters and statistical analysis.

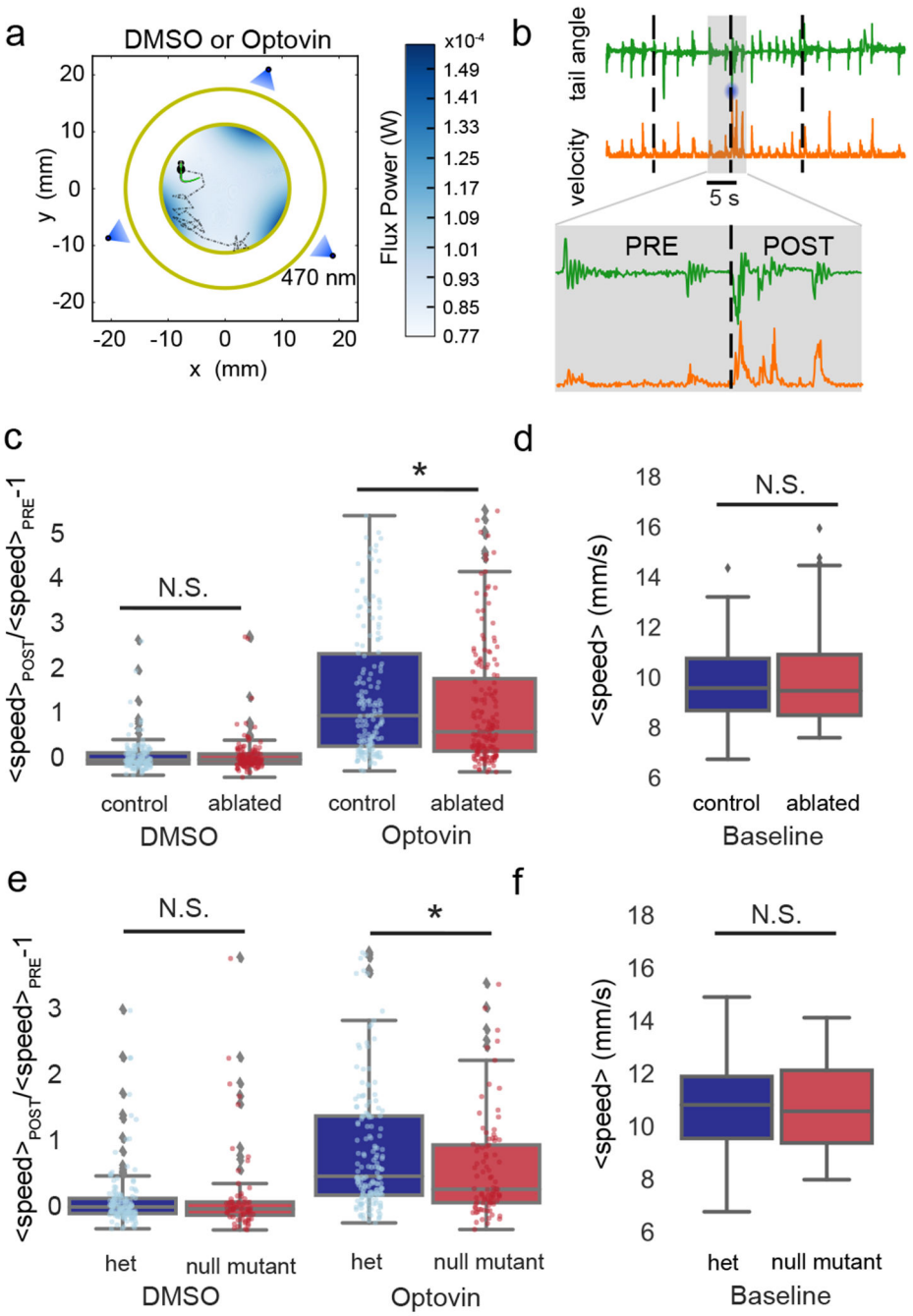

Figure 8: Loss of OXT function attenuates behavioral responses to TRPA1 activation

(a) Schematic of the free-swimming TRPA1 stimulation behavioral setup.

(b) Bottom: A representative example of the head velocity (mm/s, orange) and cumulative tail angle (°, green) of a fish before and after light stimulation (blue circle) in Optovin solution. All of the response parameters were computed in the 5 s pre- and post-stimulus time windows. Bottom: Higher magnification images of the gray highlighted area.

(c) Chemical-genetic ablation of OXT neurons reduces responses to TRPA1 stimulation. While MTZ-mediated ablation of OXT neurons did not affect behavior in DMSO (p=0.93,

$n_{control}$=141 stimulations from 44 fish, $n_{ablated}$= 137 stimulations from 44 fish, two-sided Wilcoxon Rank Sum test), in Optovin the response of ablated fish was 35% lower than for MTZ-treated sibling controls (*p=0.024, $n_{control}$ = 162 stimulations from 44 fish, $n_{ablated}$ = 175 stimulations from 44 fish). Blue = MTZ-treated control, Red = ablated. Box plots from (c) – (e) shows median, interquartile range and entire data range excluding outliers. Outliers are depicted by gray diamonds.

(d) Comparison of baseline swim speeds between MTZ-treated control and ablated fish (p=0.77, two-sided Wilcoxon Rank Sum test). The baseline kinematics were calculated for the 3 min period prior to the first stimulation in the DMSO condition.

(e) Genetic deletion of *oxt* reduces responses to TRPA1 stimulation. While light flashes were equally ineffective at eliciting responses for both genotypes in DMSO (p = 0.29, n_{het} = 145 stimulations from 45 fish, n_{null} = 69 stimulations from 26 fish, two-sided Wilcoxon Rank Sum test), in Optovin the response of the mutants was 38% lower than for heterozygous controls (*p=0.015, n_{het}= 160 stimulations from 45 fish, n_{null} = 89 stimulations from 26 fish). Blue = heterozygous siblings, Red = null mutants.

(f) Comparison of baseline swim speeds between heterozygous and null mutants (p=0.92, two-sided Wilcoxon Rank Sum test). The baseline kinematics were calculated for the 3 min period prior to the first stimulation in the DMSO condition.